Finite Element Based Microstructural Modeling of Cementitious Composites

by

Amit Maroli

A Thesis Presented in Partial Fulfillment
of the Requirements for the Degree
Master of Science

Approved April 2016 by the
Graduate Supervisory Committee:

Narayanan Neithalath, Chair
Subramanium Rajan
Barzin Mobasher

ARIZONA STATE UNIVERSITY

May 2016

ABSTRACT

This study employs a finite element method based modeling of cementitious composite microstructure to study the effect of presence of inclusions on the stress distribution and the constitutive response of the composite. A randomized periodic microstructure combined with periodic boundary conditions forms the base of the finite element models. Inclusion properties of quartz and light weight aggregates of size 600μm obtained from literature were made use of to study the effect of their material (including inclusion stiffness, stiffness of interfacial transition zone and matrix stiffening) and geometric properties (volume fraction of inclusion, particle size distribution of inclusion and thickness of the interfacial transition zone) on the composite. Traction-separation relationship was used to incorporate the effect of debonding at the interface of the matrix and the inclusion to study the effect on stress distribution in the microstructure. The stress distributions observed upon conducting a finite element analysis are caused due to the stiffness mismatch in both the quartz and the light weight aggregates as expected. The constitutive response of the composite microstructure is found to be in good conformance with semi-analytical models as well as experimental values. The effect of debonding throws up certain important observations on the stress distributions in the microstructure based on the stress concentrations and relaxations caused by the stiffness of the individual components of the microstructure. The study presented discusses the different micromechanical models employed, their applicability and suitability to correctly predict the composite constitutive response.

DEDICATION

This thesis is dedicated to my parents, Anil Maroli and Indira Maroli, who have taken innumerable sacrifices in every phase of my life and have provided me with moral support and guidance throughout my academic career. Without their love, affection, support and unwavering belief in me, I would not be half the man I am.

ACKNOWLEDGMENTS

First and foremost, I would like to express my gratitude to my advisor, Dr. Narayanan Neithalath for providing me the opportunity to work with him. I am grateful to him for his valuable lessons on the fundamentals of properties of concrete. Dr. Neithalath has shown me the importance of attending to details while performing simulations. His emphasis on minute details and constant reminders to always focus on the fundamentals has helped me become an able researcher. His encouragement and support throughout the course of my masters has been a major driving force.

Secondly, I would like to thank the rest of my thesis committee, Dr. Subramanium Rajan for teaching me the important aspects of finite element analysis through my graduate studies.

I'd like to thank all my co-researchers in the Structures Laboratory at Arizona State University for their support and assistance throughout this research. I'm greatly appreciative of Sumanta Das for his invaluable inputs on understanding the fundamentals of the microstructural models.

Finally, I'd like to thank my family and my friends here and in India for their love and support especially during the difficult times.

TABLE OF CONTENTS

Page

CHAPTER Page

LIST OF TABLES

Table Page

LIST OF FIGURES

Figure Page

Figure Page

Chapter 1: Introduction

1.1 Background

Contemporary engineering applications have been significantly improved by the use of composite materials specially developed and designed to provide the preferred mechanical behavior. Some desired properties for instance are light weight, high stiffness or high flexibility, good thermal and mechanical durability, high yield strength under static or dynamic loading and good surface hardness. Usually homogeneous materials satisfy only some of the desired properties. On the other hand, composite materials can be specifically designed to bring out a variety of their most desired behaviors based on the required scope of application. This is the prime reason why interest in composite materials is ever-growing in the field of engineering, which combine the specific properties of its constituents in a highly application-oriented approach. Concrete along with fiber reinforced materials, ceramics and metal composites are some of the most versatile and widely used composite materials used in the industry having far ranging applications. Concrete which is the most commonly used construction material on earth, when considered over its entire life cycle from processing, construction, operation, demolition to recycling makes a significant contribution to the environmental, social and economic aspects of sustainable development. Concrete is a versatile construction material: it is plastic and malleable when newly mixed, yet strong and durable when hardened. These qualities explain why concrete can be used to build skyscrapers, bridges, sidewalks, highways, houses and dams. To obtain specific desired properties from concrete or to improve certain properties of concrete modification of its binder and/or the modifications of its inclusions can be taken up. The cement based mortar binder can be modified by

infusing it with flyash, alkali-activated flyash, slag, silica fume etc, which are already widely practiced for a variety of components, whereas the inclusions in the binders can themselves be replaced partially or completely by a variety of materials like rubber particles, light weight aggregates, glass beads, phase changing materials etc.

The underlying foundation of all composite materials is that their macroscopic properties are strongly influenced and determined by the properties of its micro-constituents and phenomena on the micro-scale. The description of the micro-structural phenomena leads to a better understanding of the macroscopic behavior. However, a drawback to the use of micro-heterogeneous materials could be that heterogeneities within the microstructure cause local stress concentration, which is often responsible for inelastic material behavior, damage and debonding of the inclusions from the matrix material. As such, it is essential to know about these phenomena and to evaluate their influence on the macroscopic behavior of the composite itself. However, most often the exact microstructure is not known, so in general some statistical assumption has to be made. The macroscopic properties are determined by a homogenization process which yields the effective stresses and strains acting on the effective, homogenized sample of material. This sample of material is often called statistically representative element area (REA). The goal of the homogenization process is to provide data which can be used to find a material model for the effective material, and to identify the parameters introduced in this material model. The effective material is supposed to represent all macroscopic properties of the micro-heterogeneous material. In general, one cannot assume the effective material model to be of the same type as the model used for the micro-constituents, which significantly complicates the search for an effective material model. Here, an exception is linear elastic

material at small strains, since the superposition principle holds for this material. Until some years ago, homogenization and the determination of effective material parameters could only be done by either performing experiments or tests with the existing material sample or by applying semi-analytical methods making rather strong assumptions on the mechanical field variables or on the microstructure of the material. Quite often, those semi-analytical methods do not lead to sufficiently accurate results. Especially for micro-constituents with extreme properties like near incompressibility, the determination of effective material parameters with the commonly used semi-analytical methods leads to considerable deviation in results from reality. Recently it is commonly accepted that numerical simulations of the microstructural behavior are necessary to get more accurate results for the effective properties of the material. These numerical simulations can significantly reduce the number of time consuming and expensive experiments with laboriously manufactured material samples. This clearly improves the development and design of new materials for modern engineering applications. One of the foremost progresses in contemporary structural components is the enhancement done on the materials to obtain the optimum behavior relevant to its application. This is done through the exploitation of the material microstructure. Composite materials have their macroscopic characteristics based on the mixture of two or more pure components like particles, platelets or fibers suspended in a binding matrix. This mixing is used in many materials like metal, concrete, polymer matrix composites, etc. In the construction of composite materials, the basic philosophy is to select material combinations to produce desired cumulative responses. For example, in aeronautic engineering applications the basic choice is a harder particulate phase that acts as a stiffening factor that adds to the

metal or polymer matrix enhanced properties against abrasion and extreme temperature-fluctuation. This suggests to carry out direct numerical simulation of microstructures and to try to establish a realistic representation of the heterogeneous structure that appends and contains all the micro-scale details. Doing so and in order to capture all the details would lead to an extremely fine spatial discretization with a very large meshes of finite elements to carry the micro-scale information. Such problems are beyond the capacity of the computational power currently available. That is why the approach of taking a small micro sample that contains a finite part of inclusions to demonstrate a "representative element area" in combination with proper boundary conditions to represent as close as possible the real composite material macro-behavior would provide us with a tool to enhance and particle understanding of the composite's material behavior based on its micro-constituents. This macro response is calculated from the micro response through a variety of methods known as numerical homogenization. Because of these essentials the use of homogenized material models is of common place in practically all branches of the physical sciences. The volume averaging takes place over a statistically representative element area (REA). The internal fields to be volumetrically averaged must be computed by solving a series of boundary value problems with test loadings [Zohdi and Wriggers 2008]. Such homogenization processes are referred to as "Numerical Homogenization", "mean field theories", "theories of effective properties", etc. For details, see [Jikov, Kozlov, and Oleinik 2012]for mathematical aspects see [Aboudi 1991; Zvi Hashin 1983; Mura 1987; Nemat-Nasser and Hori 2013] for more in-depth studies into this subject. For a sample to be statistically representative it must usually contain a sufficient number of inclusions and should have a larger size relative to the size of each inclusion. The

calculations for a REA are still large, but are much inferior in comparison with the simulation of the real structure. Historically most classical analytical or semi analytical methods for estimating the macroscopic response of such engineering materials have strongly phenomenological basis, and are in reality non-predictive of material responses that are unidentified. This is true even in the linearly elastic, infinitesimal strain range. In plain words such models require extensive experimental data to tune parameters that have little or no physical significance. The arguments about this issue have led to the computational approaches which require relatively simple description on the microscale, containing parameters that are physically meaningful or realistic. In other words, the phenomenological aspects of the material modeling are reduced, with the burden of the work being shifted to high performance computational methods. Stated clearly, the aim of computational micro-macro mechanics is to develop relationships between the microstructure and the macroscopic response of a composite material, using representative models on the microscale that are as simple as possible and provide an acceptable presentation for the composite material in investigation.

The use of the finite element method (FEM) for the micromechanical analyses of random composites, which represent most of the real composites, is very expensive from a point of view of processing time and use of computer memory. In fact, the FEM discretization of a REA with many heterogeneities involves a problem with a large number of degrees of freedom (the REA contains the heterogeneities characterizing the microstructure of the composite). Such problems have been analyzed by[Ghosh et al. 2000], who have developed a plane finite element model based on a polygonal Voronoi cell [Voronoi 1907]. Inconveniences due to the use of random distributions of inclusions

and defects can be avoided by assuming a periodic distribution of such heterogeneities. In fact, in this case it is possible to adopt an REA containing a small number of heterogeneities and equipped with suitable periodic boundary conditions. Throughout this work, the case of linear elasticity is considered. In this perspective, the mechanical properties of micro heterogeneous material are characterized by a spatially variable elasticity tensor C. Generally, in order to demonstrate the homogenized effective macroscopic response of such materials, the relation between averages turns to be

$$\sigma_{\Omega} = \mathrm{C}_{\mathrm{eff}} \,.\, \varepsilon_{\Omega} \tag{1.1}$$

and where σ_{Ω} and ε_{Ω} are the volume average stress and strain tensor fields within a REA of volume Ω. The quantity C_{eff}, is known as the effective property, and is the elasticity tensor used in usual structural scale analysis. Similarly, one can describe other effective quantities such as conductivity or diffusivity, in virtually the same manner, relating other volumetrically averaged field variables.

1.2 Objective

This work comprises a framework for finite element (FE)-models starting from micro-structure generation to the calculation of the composite material effective properties. It investigates, verifies and compares different types of REAs for spherical inclusions representing particle reinforcement. Micro-structures (REAs) are generated as geometry which are then meshed with a python script through ABAQUS™ to obtain an orphan mesh file. Periodic boundary conditions (P.B.C.) are developed to meet the intended numerical homogenization requirements. A meshing module is programmed with python language to prepare and append to the input orphan mesh file. After this stage, a targeted perturbation

is applied and the job is sent to ABAQUS^{TM} solver. A homogenization module is developed to handle the post processing stage over the outcome of the simulation. This module is responsible for calculating the composite's effective material properties in terms of the volume averaged stress and strain tensors of the REA. The framework is applied for various types of spherical inclusion-filled REAs. The main objectives of the present study can be summarized through the following points:

- Build up a micromechanical model (representative element area) for spherical-particles reinforced composite materials to be used as a useful tool to verify and evaluate existing analytical and semi-analytical material models, and to have a reliable FE-model to be used in numerical simulation experiments that replaces real experiments.
- Development of suitable boundary conditions that adhere to all the special requirements for the intended simulations and numerical homogenization.
- Establishing a homogenization process acting as a tool to determine the effective material properties of an isotropic composite material based on the matrix/filler properties and their realistic micro-geometry or structure.
- Evaluation of the influence of the phase material and geometric properties on the micro-structural stress distribution and the constitutive response of the REA in the linear elastic regime based on the matrix/filler properties and their realistic micro-geometry or structure.
- Evaluation of the influence of de-bonding of the interface between the matrix and the inclusion on the phase material and geometric properties on the micro-structural stress distribution and the constitutive response of the REA in the linear

elastic regime based on the matrix/filler properties and their realistic micro-geometry or structure.

1.3 Organization of Thesis

This thesis is primarily composed of a research paper that is submitted and another research paper that will be submitted for publication. Some chapters contain additional data that are not presented in papers. These papers are presented in Chapter 3-5. This section shows overall organization of the thesis for clarity.

Chapter 2 consists of extensive literature review on homogenization methods used and the need for numerical homogenization.

Chapter 3 discusses in detail the development of the F.E. framework which includes the theory behind generation of the randomized periodic microstructure, formulation and the application of periodic boundary conditions. This chapter gives a generalized description of the F.E framework. Detailed application-specific information on materials are detailed in individual chapters.

Chapter 4 studies the influence of phase material and geometric properties on the micro-structural stress distribution in the cement mortar and the constitutive linear elastic response of the REA.

Chapter 5 studies the influence of de-bonding at the interface between the matrix and the inclusion on micro-structural stress distribution in the cement mortar and the constitutive linear elastic response of the REA.

Chapter 2: Literature Review

2.1 Background

The link between the material microstructure and relevant mechanical properties provides valuable information towards design and development of sustainable cementitious materials for several applications. In recent years, many novel cementitious composites have emerged, incorporating several types of inclusion materials for various special applications such as the use of lightweight aggregates (LWAs) for internal curing, reduction of dead load, thermal and acoustic insulation[Al-Jabri et al. 2005; Cusson and Hoogeveen 2008; Kim, Jeon, and Lee 2012; Nguyen et al. 2014], microencapsulated phase change materials (PCM) for control of thermal cracking in pavements and bridge decks[Fernandes et al. 2014] and regulating internal environment in buildings [Hembade, Neithalath, and Rajan 2013; Thiele et al. 2015], waste and recycled materials such as rubber for energy absorption [Hernández-Olivares et al. 2002], and denser/stiffer aggregates for radiation shielding [Akkurt et al. 2006; Makarious et al. 1996]. Incorporation of such inclusions influences the individual stresses in the micro-structural components and the stress distributions in the composite, thereby dictating the failure path/mechanism of the material. Hence a comprehensive understanding of the influence of inclusion types on the micro-structural stress distribution is necessary to design such materials for desired mechanical performance. Dealing with composite materials properties is an early interest in the science of materials. Homogenization tools and methods to determine the effective material properties of composites have been developed and dealt with since late 19th century and until our times. Recently numerical homogenization approaches based on FE methods are being developed and enhanced to meet more realistic and precise results based

on the microstructure of the composite. Starting from probing the inhomogeneous material, for example in linear elastic materials to measure the Young's modulus and Poisson ratio, a sample is tested under tension and compression load tests. The stresses and strains measured are the averages for the specimen. Assuming that the material is homogeneous and the results are the effective properties of this material while in reality there is no such a homogeneous material. Even at the micro scale when two phases are analyzed, one should always assume that each phase is homogenous by itself which is not the case in reality since even pure material components are inhomogeneous at a certain scale. So the assumption of homogenization is always taken when using any type of material properties' predictions, whether using empirical, analytical, semi-analytical or numerical FE-based methods.

2.2 Homogenization techniques

Some of the early studies on the concept of homogenization of heterogeneous microstructures were done more than a century ago by [Voigt 1889] and [Reuss 1929] who both proposed different simple approximations for the effective material data of heterogeneous linear elastic materials, which have been the basis for a primary result by [Hill 1952]. The Voigt and Reuss assumptions have a physical interpretation as being displayed in Figure 2.1. Looking at a rod under a tension load the Voigt approach would be exact for different materials being connected in parallel relative to the applied load. The Reuss model would be exact for different materials being connected in series.

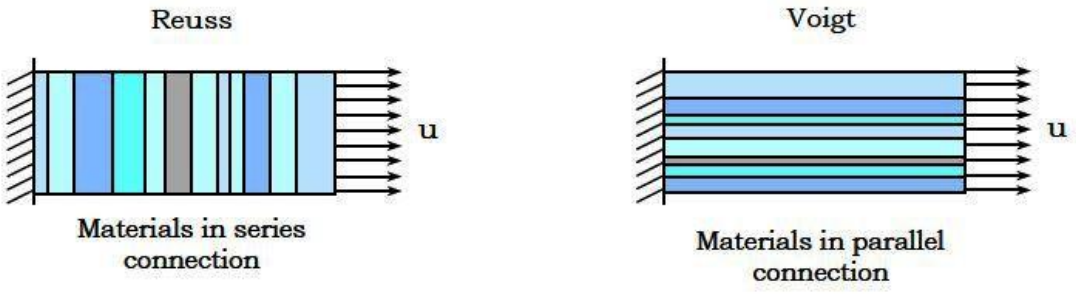

Figure 2.1. Geometrical Interpretation of Reuss and Voigt theoretical bounds

Regarding Voigt bound, it corresponds to the assumption that the inclusion and the matrix both experience the same uniform strain. Then the average strain tensors of the inclusion and matrix are equal to the composite average strain $\varepsilon^I = \varepsilon$, so the following expression for the stiffness tensor is given by [Tucker III and Liang 1999],

$$C^{Voigt} = C^m + V_I(C^I - C^m) = V_I C^I + V_I C^m \tag{2.1}$$

This leads to the representation of the Voigt upper bound (or the rule of mixtures) of the effective stiffness of the composite. On the other hand, Reuss assumes that the inclusion and matrix experience same uniform stress. The compliance tensor is given by [Tucker III and Liang 1999],

$$S^{Ruess} = S^m + V_I(S^I - S^m) = V_I S^I + V_I S^m \tag{2.2}$$

This leads to the representation of the Reuss lower bound of the effective stiffness of the composite.

More tight bounds for linear elasticity were proposed by Hashin and Shtrikman (1962), (1963). Hashin and Shtrikman bounds are based on variational principles. They engage the principle of minimum potential energy and the principle of minimum complementary potential energy. The bounds for the material parameters of an isotropic

linear elastic effective material consisting of two phases with volume fractions V_1 and V_2 and material parameters K_1 , K_2 , μ_1 and μ_2 , respectively are described in [Zohdi and Wriggers 2008] and [Löhnert 2004]. The Hashin and Shtrikman bounds are only asymptotic bounds and strictly valid only for a theoretically infinite size of the representative volume element they are used for. But they are the tightest possible bounds for general isotropic materials without restrictions on the geometry of the microstructure[Löhnert 2004].

The introduction of the Eshelby model middle of the 20th century is one of the major achievements in the analytical approach for predicting the effective material properties of heterogeneous microstructures besides the previously mentioned bounds. Many models are based on this analysis going back to the work of Eshelby (1957) who found a general solution for one ellipsoidal particle embedded in an infinite matrix in linear elasticity. Eshelby (1957) found that for a homogeneous isotropic infinite body with an ellipsoidal inclusion subjected to a uniform eigen strain ε^*, the resulting strain field within the inclusion is uniform and can be described by,

$$\varepsilon = \xi - \varepsilon^* \tag{2.3}$$

where ξ is the called the fourth rank Eshelby tensor. It only depends on the geometry of the ellipsoidal inclusion and poisson's ratio. Eshelby's model can be used to predict the effective stiffness of a composite with ellipsoidal inclusions at dilute concentrations. That is why it is sometimes called the dilute Eshelby's model. Note that the average strain is identical to the applied strain ε^A [Tucker III and Liang 1999]

$$\varepsilon = \varepsilon^A \tag{2.4}$$

Therefore the relation between the average composite strain and the average inclusion's strain is

$$\varepsilon = \varepsilon^I[I + \xi S^m(C^I - C^m)] \tag{2.5}$$

For a representative formulation of the above equation, see[(Tucker III and Liang 1999)]. Therefore we get,

$$\varepsilon^I = A^{Eshelby}\varepsilon \tag{2.6}$$

Therefore,

$$A^{Eshelby} = [I + \xi S^m(C^I - C^m)]^{-1} \tag{2.7}$$

This form will be later used for the derivation of Mori-Tanaka's models, which are based on Eshelby's model.

The Mori-Tanaka (MT) model was proposed by Mori and Tanaka (1973) and it is suited for composites with moderate inclusion volume fraction. For details on formulation and numerical implementation see [Doghri and Ouaar 2003]. Mori-Tanaka's assumption was that when many identical particles are introduced to the composite microstructure, the average inclusion strain is given by

$$\varepsilon^I = A^{Eshelby}\varepsilon^m \tag{2.8}$$

This means, within a concentrated composite each single inclusion sees a far field strain that is equal to the average strain of the matrix rather than the composite as in Eshelby's case (See eqn. 2.6). Here one obtains the Mori-Tanaka strain concentration tensor, which can be used to calculate the overall effective stiffness tensor of the composite.

The double inclusion model (DI) was proposed by [Nemat-Nasser and Hori 2013] supposes that each spherical inclusion of stiffness C^I is wrapped with a matrix material of stiffness C^m. The outer reference material has a stiffness C^R. The composite has an average

or effective stiffness C^{eff}. For details on formulation and numerical implementation see [Doghri and Ouaar 2003]. By choosing the surrounding reference stiffness C^R to be either the matrix, inclusion's or the effective composite's stiffness; one can retrieve many homogenization models. The choice $C^R = C^{eff}$, means that the inclusion is surrounded by a material having the effective stiffness of the whole composite, gives the generalized self-consistent model. A second choice is $C^R = C^m$, the stiffness of the real matrix material gives the Mori-Tanaka model, thus describing a lower bound for the alternate concentration tensor on the presumption that the inclusion is stiffer than the matrix. A third choice of $C^R = C^I$, the stiffness of the real inclusion. This means that the matrix is stiffer and engulfing a softer material of the inclusion. This case can be called the inverse MT model, as it corresponds to MT for a composite where the material properties of the inclusion and the matrix are permuted. This describes the upper bound since the reference is taken to be the stiffer material of the inclusion. Note that ξ^I is now calculated for inclusions of matrix material and surrounded by the inclusion material, i.e. inversed.

Several such homogenization methods have been developed over the years and classical references on heterogeneous materials can be found, for example, in[Eshelby 1957; Weng 1984; Hubert and Palencia 1992; Nemat-Nasser and Hori 2013]. Specific references about multiscale approach on cement based material are available in[Z. Hashin and Monteiro 2002a; Grondin et al. 2007; Dormieux, Kondo, and Ulm 2006; Sanahuja, Dormieux, and Chanvillard 200)]. Some authors have also proposed to use micromechanical schemes to predict the failure strength of concrete, as the Mori–Tanaka approach [C. C. Yang and Huang 1996b]. Note that the macroscopic response of particle reinforced composites is influenced by not only the component properties and component

concentrations, but also the interfacial interaction between the particles and the matrix and interfacial debonding. In particular, the inclusion of stiff particles to a soft matrix can lead to an increase in composite stiffness, strength, impact resistance, and abrasion resistance[Leblanc 2009; Leblanc 2002]. Additionally, at large deformations particles tend to debond from the matrix, influencing both the ductility and fracture toughness of the composite [Qiao 2003; Segurado and LLorca 2004; Kitey and Tippur 2005]. Debonding is characterized by a localized region of failure (or interfacial debonding) that accumulates around the particle inclusions. On the other hand, as a result of chemical interactions, an interphase may form between the particle and the matrix during manufacturing and processing. Even though these interphases are typically microscopic, they can greatly influence the macroscopic behavior of composite materials. The extent and composition of this interphase depends on a number of factors, including the surface area and surface treatment of the particles, as well as the level of mixing and age of the composite[Leblanc 2002]. In contrast to the numerous experimental investigations, there have been few theoretical investigations which consider the effect of either interphases or interfacial debonding in the finite deformation regime. One of the few formulations for debonding under finite strains was presented by [Brassart et al. 2009]. They extend the Mori–Tanaka homogenization scheme [Mori and Tanaka 1973a] to account for the debonding of composite materials under finite strains; however, they do not account for the presence of interphases. More recently, [Goudarzi et al. 2015] presented a theoretical framework capable of describing the influence of interphases on the macroscopic constitutive response of particle reinforced elastomers. They compare their formulation to both numerical and experimental results[Ramier 2004], and found excellent correlation with both. However,

their investigation focuses on the influence of perfectly bonded interphases, excluding the consideration of interfacial debonding. There are four primary factors which influence the macroscopic constitutive response of particle reinforced composites: component properties, component concentrations, interphases, and interfacial debonding. This thesis presents a computational framework capable of capturing the influence of interphases and interfacial debonding on the finite deformation response of particle reinforced composites. The influence of the thickness and modulus of the interphase is considered, and debonding is accounted for by incorporating bi-linear traction separation relation.

2.3 Numerical Homogenization

The limitations faced when using analytical approximation methods make direct numerical simulations necessary. Therefore, during the last years numerical methods to directly compute the effective material data gained more and more interest and importance. Most of those methods are developed only for linear material laws and small deformations. Just recently and due to the increasing computational power available, a couple of methods for non-linear elasticity and general non-linear material behavior have been developed [Löhnert 2004]. Theoretical work has been done by [C. Huet 1982; C Huet 1990; Torquato 1991]. [Zohdi and Wriggers 2001a; Zohdi and Wriggers 2001b] have worked on computational homogenization of geometrically linear and possibly materially non-linear microstructures. Homogenization at finite strains and possibly inelastic material behavior has been done by [Schröder 2000; Miehe, Schröder, and Becker 2002; Miehe 2003]. This approach yields a load dependent effective material tangent stiffness and this way is applicable to multi-scale methods.

The average strain theorem states that for any perfectly bonded material within the REA and for an exterior homogeneous displacement given on the entire boundary of the REA, the volume average of the strain is the applied displacement on the boundary. For details on the theory and derivation see [Löhnert 2004]. The average strain theorem states that for any perfectly bonded material within the REA and for an exterior homogeneous displacement given on the entire boundary of the REA, the volume average of the strain is the applied displacement on the boundary [Löhnert 2004].

In an attempt to elucidate the influence of stiffness of inclusions on the distribution of stresses in the different phases in cementitious systems, this study employs a microstructure-guided micromechanical modeling scheme using the finite element method. Traditionally, the influences of inclusion type and stiffness on the mechanical behavior(elastic modulus, strength) of cementitious systems are evaluated experimentally[Bogas and Gomes 2013; Cheeseman and Virdi 2005; J. M. Chi et al. 2003], or through analytical approaches such as Mori-Tanaka [Nilsen, Monteiro, and Gjørv 1995; C. C. Yang 1997; C.-C. Yang and Huang 1998] and double inclusion [Stora, He, and Bary 2006; C. C. Yang and Huang 1996a]models or iterative homogenization techniques[Ke et al. 2010; Zouari, Benhamida, and Dumontet 2008]). Analytical homogenization techniques have been shown to provide good estimates of the effective property of cementitious systems [Das et al. 2015; Dunant et al. 2013].However, these analytical and semi-analytical homogenization techniques do not have the capability to evaluate local stress concentrations around inclusions which influence the macroscopic behavior, especially for cementitious systems that exhibit heterogeneity at a microscopic scale. Thus, microstructure-guided numerical modeling is a favored approach under such

considerations. A few recent studies have evaluated stress localization in the lightweight aggregate-matrix interface using an analytical approach [Ke et al. 2014] or through a macroscopic numerical simulation of a compression test [Malachanne et al. 2014], thus helping to understand the effect of soft inclusions on mechanical properties. In this thesis, 2D periodic microstructures for mortars containing spherical quartz (stiff) or lightweight aggregate (soft) inclusions, including the interfacial transition zone (ITZ) around inclusions, are generated virtually and the representative element areas (REA) thus obtained are numerically analyzed using finite elements by invoking periodic boundary conditions [Li 2008; van der Sluis et al. 2000; Xia et al. 2006].The fundamental differences in stress distributions in the microstructure as a function of the inclusion type, and the relative efficiency of matrix and interface stiffening are clearly brought out. In addition, the constitutive relationships in the linear elastic regime (considering in-service performance of structures) are also evaluated for both the material systems considered. Such comprehensive numerical evaluations of fundamental differences in local micro-stress distributions imparted by differences in inclusion type, and its resultant influence on the macro scale mechanical response are rather uncommon.

Chapter 3: Finite Element Based Framework for Microstructural Stress Analysis and Prediction of Young's Modulus

In a numerical simulation, it is unnecessary and not efficient to simulate everything we encounter, especially when there are reliable analytical models that sufficiently describe and solve the task. Generally, we choose a region of interest in which we conduct a numerical simulation where limitations of analytical models exist. The interesting region has a certain boundary with the surrounding environment. Numerical simulations therefore have to consider the physical processes in the boundary region by appropriately chosen boundary conditions (BC). Different boundary conditions may cause quite different simulation results. Improper sets of boundary conditions may introduce nonphysical influences on the simulation system. So arranging the boundary conditions for different problems becomes very important. While at the same time, different variables in the environment may have different boundary conditions according to certain physical problems. Generally speaking, boundary conditions represent the type and value of constraints that control the simulation response of our microstructure (RVE) and their usage is dependent on the type of the RVE used due to the various geometric possibilities in generating them.

3.1 Microstructure Generation and the Modeling Scheme

This section describes the microstructure-guided constitutive modeling framework for heterogeneous materials. The framework explained herein executes multi-scale analysis of heterogeneous materials involving generation of a unit cell based on known inclusion size distributions, meshing of the unit cell and application of appropriate boundary

conditions, and microstructural stress analysis. The detailed procedure is explained in the following sub-sections.

3.2 Generation of Representative Element Area (REA)

Generation of REA is accomplished here using the Lubachhevsky-Stillinger algorithm [Lubachevsky and Stillinger 1990a; Lubachevsky 1991a; Lubachevsky, Stillinger, and Pinson 1991a; Meier, Kuhl, and Steinmann 2008a]. This algorithm employs non-overlapping particles on a rectangular REA. First, the desired number of particles are randomly distributed inside the periodic bounding box with random initial velocities of the particles. The radius of each particle is initialized as zero. The radius of i^{th} particle (r_i) in the next event is a function of the growth rate (g_i), which is tailored to attain the desired particle size distribution, as shown in Equation. 3.1.

$$\frac{dr_i}{dt} = g_i \tag{3.1}$$

The growth rate between time t^n and t^{n+1} is computed using a finite difference scheme as follows:

$$g_i = \frac{(r_i^{n+1} - r_i^n)}{\Delta t} \tag{3.2}$$

The particle radii are then updated using the growth rate and time increment. The position of particle "i" is also updated considering a constant velocity between time nodes. Checks for particle contacts and post-contact velocities are made in each time step, and all particle positions are updated using a forward Euler scheme. These steps are repeated and in the process of iterations the particles change position in the bounding box, collide and grow in order to obtain the desired volume fraction. Finally, the obtained microstructural

information is scripted in python language to be imported to ABAQUS^{TM} for finite element implementation. More details on the microstructure generation algorithm can be found in [Lubachevsky and Stillinger 1990a; Lubachevsky 1991a; Lubachevsky, Stillinger, and Pinson 1991a; Meier, Kuhl, and Steinmann 2008a].

Within the Lubachevsky–Stillinger algorithm, the generation of a representative volume element is accomplished by employing an event-driven scheme advancing from event to event, see[Lubachevsky and Stillinger 1990b; Lubachevsky 1991b; Lubachevsky, Stillinger, and Pinson 1991b]. Here, an event is considered to be the discrete collision between two particles. Each event is considered individually and in serial, postulating that only one discrete event is taking place at one discrete time. This leads to the possibility to handle each event individually. The basic steps of finding and handling an event are specified in Sections 3.2.1 and 3.2.2, whereas the algorithm used to produce the REA is described in Section 3.2.3.

3.2.1 Event-driven time step calculation

In an event-driven scheme, the particles evolve independently at all time except for discrete asynchronous instances of pair-wise interactions. The time step size is thus governed by the sequence of events. To calculate the time step Δt which is needed to advance the particle system from time t^n (Figure 3.1, left) to time t^{n+1} (Figure 3.1, right) the event, collision between two particles, has to be observed. Since we are using a hard contact model we do not allow for particle overlap. Entering at time t^n we assume that the positions of the particle centers $\mathbf{x}^n{}_i$, the particle radii $r^n{}_i$ as well as the particle velocities $\mathbf{v}^n{}_i$ are known. The key idea of the present REA generation scheme is that the initial individual particle radii are set to zero such that *ab initio* the particles are not in contact.

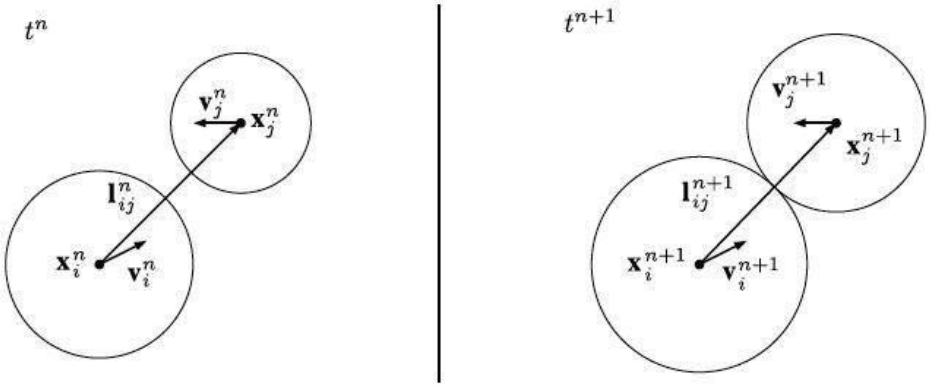

Figure 3.1. Configuration of particle *i* and *j* at time *tn* prior to contact and at *tn*+1 defining the time step size Δ*t* due to the event 'particles in contact'.

The particle radii r_i are then assumed to increase as

$$\dot{r}_i = g_i \quad \forall\, i \in \{1, \ldots\ldots, nop\} r_i, g_i \in R \tag{3.3}$$

The volume fraction Φ, i.e. the volume occupied by the particles per volume of the periodic boundary box is thus controlled by the growth rate g_i. If g_i is equal for all particles *i*, a monodisperse packing is constructed, while different growth rates g_i generate a multi-disperse packing, see [Kansal, Torquato, and Stillinger 2002]. The discrete counterpart of (3.3) can be constructed, e.g. with the help of a finite difference scheme, i.e. $\dot{r}_i \approx [r^{n+1}{}_i - r^n{}_i]/\Delta t$, yielding the discrete update equation of the particle radii at time t^{n+1}:

$$r^{n+1}{}_i = r^n{}_i + g_i \Delta t \qquad \forall\, i \in \{1 \ldots\ldots, nop\} \tag{3.4}$$

Postulating a constant velocity of particle *i* between the time nodes, the position of particle *i* at time t^{n+1} is calculated by using the well-known forward Euler formula:

$$x^{n+1}{}_i = x^n{}_i + \Delta t v^n{}_i \quad \forall\, i \in \{1, \ldots\ldots, nop\}, \qquad x_i, v_i \in R^{dim} \tag{3.5}$$

The branch vector $\mathbf{l}^{n+1}{}_{ij}$ which connects the centers of the particles *i* and *j* is calculated by

subtracting the position vectors of the particles:

$$l^{n+1}{}_{ij} = x^{n+1}{}_j - x^{n+1}{}_i \quad \forall\, i \neq j, \quad i,j \in \{1,\dots,nop\} \tag{3.6}$$

For the sum of the particle radii being equal to the length of the branch vector, $\|\mathbf{l}^{n+1}{}_{ij}\| = r^{n+1}{}_i + r^{n+1}{}_j$, particles *i* and *j* are in contact, see Figure 3.1, right. Using (3.4) and (3.5) we can define the relevant time step size for the event-driven scheme Δt

$$\Delta t = \min_{\Delta t>0}\left\{\frac{[-v \pm \sqrt{v^2-uw}\,]}{u}\right\} \tag{3.7}$$

with

$$v = l^n{}_{ij} \cdot \left[v^n{}_j - v^n{}_i\right] - \left[r^n{}_i + r^n{}_j\right][g_i + g_j] \tag{3.8}$$

$$u = \left[v^n{}_j - v^n{}_i\right]^2 - [g_i + g_j]^2 \tag{3.9}$$

$$w = l^n{}_{ij}{}^2 - \left[r^n{}_i + r^n{}_j\right]^2 \tag{3.10}$$

The minimum of the two possible solutions for all possible particle contacts of the system defines the first contact and thus the time needed to advance to the next event.

3.2.2 Event handling

Being able to advance to the next event, the event itself has to be handled. Contact will be treated as a purely elastic impact between two bodies of equal mass. By taking into account the additional increase in size of the two colliding particles, the relation between the particle normal velocities directly before and right after the collision can be formulated as

$$v^{n+1^+}{}_{n_i} = min\left\{v^{n+1^-}{}_{n_i}, v^{n+1^-}{}_{n_j}\right\} - g_i, v^{n+1^+}{}_{n_j} = max\left\{v^{n+1^-}{}_{n_i}, v^{n+1^-}{}_{n_j}\right\} + g_i \tag{3.11}$$

in terms of the growth rate g_i and the normal contact velocity

$$v^{n+1}{}_n = v^{n+1} \cdot n^{n+1}{}_{ij} \text{ with } n^{n+1}{}_{ij} = \frac{l^{n+1}{}_{ij}}{||l^{n+1}{}_{ij}||} \tag{3.12}$$

Herein, $(\bullet)^-$indicates quantities prior and $(\bullet)^+$posterior to the collision. The assumption of the smoothness of the particles leaves the tangential particle velocities unchanged.

3.2.3 Event-driven generation of the REA

For simplicity, the REA is set to be a square with dimensions $l_{rea} \times l_{rea}$; however, any reasonable shape is possible. The desired number of particles is randomly distributed inside the periodic boundary box, initialized with random particle velocities. Radii of all particles are set to zero. Of interest is the next particle pair collision and its time. The time step calculation outlined in Section 3.2.1 is performed for each particle pair being able to collide. Different algorithms for fast collision detection can be found in the literature [Munjiza 2004]. We use a parallelized screening contact detection algorithm, the search time is of the order *∂(*number of particles*)*. The minimum time step of all possible collisions, calculated by (3.7), is selected to advance the event-driven scheme. Next, all particle positions $\mathbf{x}^{n+1}{}_i$are updated in terms of a forward Euler scheme (3.5). The post contact velocities of the colliding particle pair are determined according to (3.11), followed by a new search for the next collision. Allowing the algorithm to take its course, the particles float around inside the rea, collide and grow depending on the elapsed time. Postulation of a dropout criterion can be accomplished in many ways. We select the increase of volume fraction

$$\Delta\phi = \phi^{n+1} - \phi^{n+1-c} \qquad \text{with} \quad \phi^{n+1} = \frac{v^{n+1}{}_{par}}{v_{rea}} = \frac{\pi}{v_{rea}} \sum_{i=1}^{nop} r^{n+1^2}{}_i \qquad (3.13)$$

to be the variable of interest. With $\Delta\Phi$ dropping under a certain threshold over a specified number of events, *c* fulfils our criterion. The complete algorithm is listed in Figure 3.2.

INITIALIZATION random positions $\mathbf{x}_i^0$, random velocities $\mathbf{v}_i^0$, radii $r_i^0 = 0$, growth rates $g_i \in \mathrm{R}$	
REPEAT	
	select minimum collision time of all possible collisions (5)
	advance all particle positions regarding the minimum collision time (3)
	update velocity of colliding particle pair (9)
UNTIL $\Delta\phi < \Delta\phi^{\mathrm{crit}}$	

Figure 3.2. Basic algorithm to produce dense particle packing by using a periodic boundary box. The dropout criterion, regarding the REPEAT UNTIL loop, is based on the increase of the volume fraction ΔΦ, see (3.13).

3.3 Boundary Conditions

Choosing appropriate microscopic boundary conditions is an essential step in any numerical stress analysis procedure. In micromechanics, the commonly adopted boundary conditions are: essential boundary conditions where uniform displacements are applied at the boundaries, or Neumann boundary conditions where uniform tractions are prescribed at the boundaries of the unit cell. These boundary conditions have been applied to predict effective properties of several materials including cementitious binders[Wriggers and Moftah 2006b; Christian Huet 1999; Ostoja-Starzewski 1999]. Since it is difficult to realize uniform boundary conditions in experimental setups, mixed boundary conditions are also proposed [Hazanov and Huet 1994; Hazanov 1998]. In this work, periodic boundary condition is adopted since it has been shown to provide better approximations of effective properties of heterogeneous materials even with relatively smaller REAs that are favorable for computational expediency[Terada et al. 2000; van der Sluis et al. 2000].

Two-dimensional plane strain microstructural finite element models are employed here in order to examine the influence of inclusion and matrix properties on the bulk elastic behavior of the composite system. A sufficiently large (4.15 mm x 4.15 mm) representative element area (REA) has been considered for the analysis. The spatial distribution of inclusions and the chosen boundary conditions play an important role in any numerical stress analysis procedure [Li 2008; van der Sluis et al. 2000]. The choice of boundary conditions as well as the spatial distribution of inclusions need to be thoroughly investigated since the boundary conditions are applied on the REA and the averaged response of REA is used as an indicator of the influence of the microstructural phases. Hence, this section investigates the effect of different boundary conditions and distribution of inclusions (in the REA) on the stress distribution in order to establish the appropriate parameters for detailed studies. In this paper, dominant principal stress (σ_{22} in this case) is taken as the microstructural stress measure[Malachanne et al. 2014].

3.3.1 Regular arrays and essential boundary conditions

In many numerical stress analysis simulations of matrix-particulate inclusion composites (such as mortar or concrete), the actual material is simplified into a model that considers either a single spherical inclusion and the matrix surrounding it [Gilabert, Garoz, and Van Paepegem 2015; Lee, Jin, and Kang 2014] or a uniform array of spherical (or circular, in 2D) particles in a continuous matrix [Drago and Pindera 2007; Jiang, Jasiuk, and Ostoja-Starzewski 2002]. The single inclusion case is generally applicable for low concentrations of particles (dilute limit). Figure 3.3(a) shows a quarter model containing a uniform array of particles with essential (displacement) boundary conditions [Ainsworth 2001]applied at the left and bottom edges, considering symmetry. The REA contains

circular quartz particles (aggregates) arranged in a square lattice within a cement paste matrix, and contains 50% inclusions. The interfacial zone around the aggregates are also accounted for. The top face of the geometry is subjected to uniform compressive loading parallel to the Y-axis. The analysis is performed using ABAQUS^{TM}. Figure 3.3(b) shows the stress distribution in the REA for an applied external stress of 40 MPa. While this configuration results in concentration of stresses at the top face due to direct application of load, the stress concentrations at the left and bottom edges are avoided due to the effective clearance between the inclusions and the boundaries. Moreover, when considering a heterogeneous material such as cement mortar, such a perfectly ordered regular lattice structure of inclusions fails to capture the randomness of particle distribution and the resultant stress distributions. This limits the application of such models for the case of random particulate composites even when the assumption of homogeneity can be applied to the global microstructure.

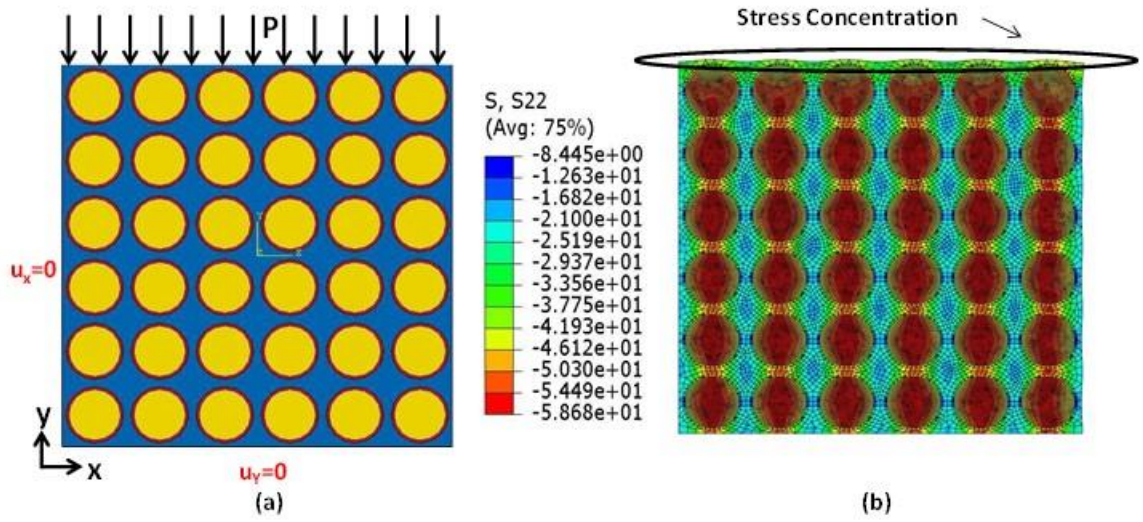

Figure 3.3. (a) FE model showing the essential boundary conditions at the edges and applied compressive loading for a regular lattice of inclusions containing interfacial zones around them. The model contains 50% of inclusions by volume (or area); (b) effect of regular inclusion distribution on the stress distribution under the boundary conditions shown and an external stress of 40 MPa. The average REA stress is 36.97 MPa (compression, shown by the negative sign of $\sigma 22$).

3.3.2 Improvements through the use of periodic microstructure and periodic boundary conditions

The limitations discussed above necessitate improvements in the model formulation with respect to the geometrical features of the microstructure where the spatial randomness in particle distribution is considered. Figure 3.5(a) shows such an improved model. Instead of having structured array of inclusions in the microstructure, we aim at generating a more realistic geometrically periodic REA. Its construction typically starts with the definition of a periodic boundary box, see Figure 3.4. Topologically speaking, the periodic boundary box for two-dimensional systems can be thought of as a torus with particles moving on the torus surface. The torus is set up by connecting the opposite boundary box sides. A particle with its center being inside the boundary box is considered to be a primary particle. If a primary particle intersects with a boundary of the periodic

boundary box, a replica of this particle is positioned on the opposite side. All properties of the primary particle are projected onto the replicated particle. As soon as the center of the primary particle leaves the boundary box, the replicated particle center enters the boundary box and their states change. This leads to a constant number of primary particles inside the periodic boundary box. The periodic boundary box is used as a frame for the periodic REA.

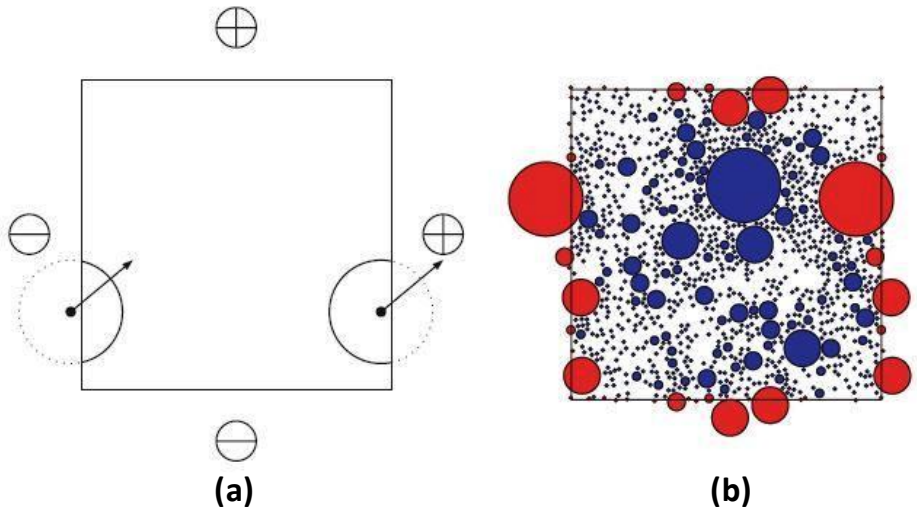

Figure 3.4. (a)Schematic illustration of a periodic boundary box including one primary particle and its replica. (b)Computational realization including primary and replica particles.

The virtual random periodic microstructure is generated using a microstructural stochastic packing algorithm[Kumar et al. 2013; Meier, Kuhl, and Steinmann 2008a; Torquato 2013]. This algorithm requires the particle size distribution (PSD) and the volume fraction of particles as inputs and it packs the circular inclusions with an interface layer of predefined thickness around them inside a REA of 4.15 mm x 4.15 mm. Generation of particles and their packing in the REA is allowed if the minimum distance between the centroids of neighboring particles is always greater than the sum of their radii., i.e., the interfacial zones are allowed to overlap in this packing scheme. Generation and random spatial placement

of inclusions goes on simultaneously until the target volume fraction of inclusions is reached. The algorithm is described in detail in [Meier, Kuhl, and Steinmann 2008a]. Note that Figure 3.5(a) shows only single size inclusions even though multiple sizes, based on inclusion PSD can be incorporated, which is implemented in a forthcoming section. After the generation of the microstructure, the REA is meshed using a Python script [Van Rossum and others 2007] through ABAQUS^{TM} and thus an orphan mesh file is obtained. Similar boundary conditions and loading as in the previous case (Figure 3.3) are applied.

Figure 3.5(b) shows the dominant principal stress (σ_{22}) distribution in the REA. The stresses in the inclusions are similar to that in the case of regular arrangement (Figure 1(b) – the color coding is different from that in Figure 3.3(a) because of extremely high stress concentrations in this case). However, the magnitude of the concentrated stresses are much higher in the regions where the inclusions intersect the edges of the REA. This artifact created by the intersection of particle with the REA boundaries are addressed as described below.

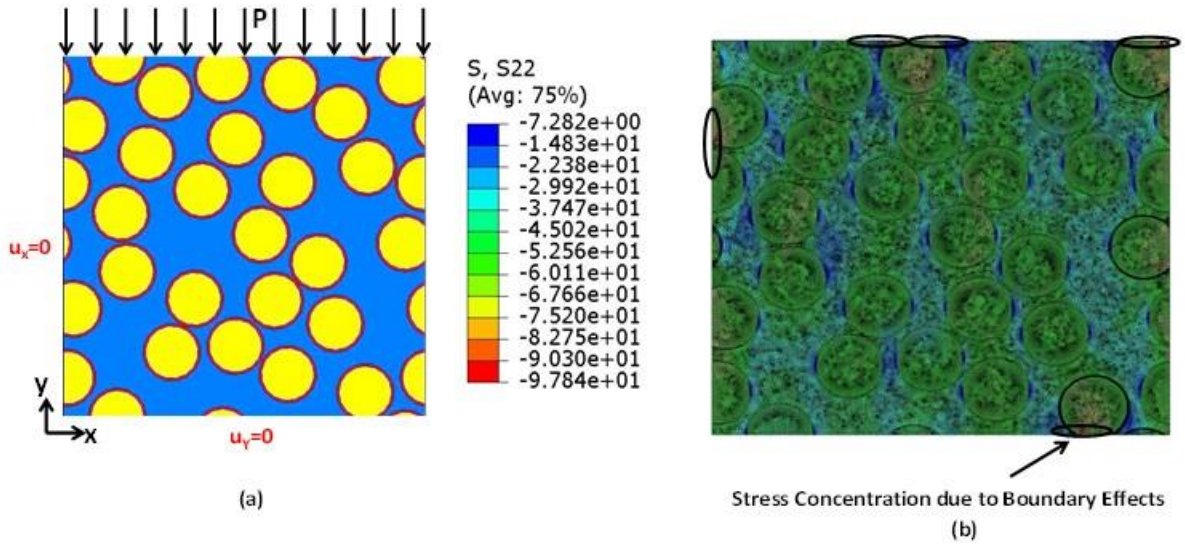

Figure 3.5. Model-II: (a) FE model showing the essential boundary conditions at the edges and applied compressive loading for a randomized spatial distribution of inclusions containing interfacial zones around them. The model contains 50% of inclusions by volume (or area); (b) effect of random spatial distribution of inclusions on the stress distribution under the boundary conditions shown and an external stress of 40 MPa. The average REA stress is 37.2 MPa

In order to eliminate the boundary effects, periodic boundary conditions[Li 2008; van der Sluis et al. 2000; Xia et al. 2006] are employed in the 2D REA as shown in Figure 3.6. Figure 3.6(a) shows schematic periodic arrays of repetitive unit cells and Figure 3.6(b) shows the periodic boundary conditions applied on one of such schematic representative elements for illustration. Periodic boundary condition ensures two continuity criteria at the boundaries of neighboring unit cells in order to ensure assembly of individual unit cells as a physical continuous body [Suquet 1987]: (i) displacement continuity, i.e., neighboring unit cells cannot be separated or they cannot penetrate each other; and (ii) traction continuity at the boundary of neighboring unit cells. The displacement field in any 2D periodic microstructure is given as:

$$v_i(x_1, x_2) = \varepsilon_{ij}^0 x_j + v_i^*(x_1, x_2) \tag{3.14}$$

Here, $\varepsilon_{ij}^{0}$is the applied strain tensor, and $v_i^*$is a periodic function representing the modification of linear displacement field due to the heterogeneous microstructure. Figure 3.6 shows a schematic representation of periodic boundary conditions. For the unit cell shown in Figure 3.6(b), the displacements on a pair of parallel opposite boundary edges are given as:

$$v_i^{s+} = \varepsilon_{ij}^{0} x_j^{s+} + v_i^* \tag{3.15a}$$

$$v_i^{s-} = \varepsilon_{ij}^{0} x_j^{s-} + v_i^* \tag{3.15b}$$

Here, s^+ and s^- are sth pair of two opposite parallel boundary surfaces of the unit cell. The periodic function v^* is the same at both the parallel opposite edges due to periodicity. The difference between the displacement fields of the two opposite parallel boundary edges is given as:

$$v_i^{s+} - v_i^{s-} = \varepsilon_{ij}^{0}(x_j^{s+} - x_j^{s-}) = \varepsilon_{ij}^{0}\Delta x_j^{s} \tag{3.16}$$

For a pair of opposite parallel boundary edges, Δx_j^s is constant for a specifiedε_{ij}^{0}. The perturbation is introduced into the system of equations through a reference node which only acts as a carrier for the load and is not attached to any element in the model. The general form of complete set of equations can be written as:

$$v_i^{s+} - v_i^{s-} + v_i^{dummy} = 0 \tag{3.17}$$

Such equations are applied as nodal displacement constraints in the finite element (FE) microstructural analysis.

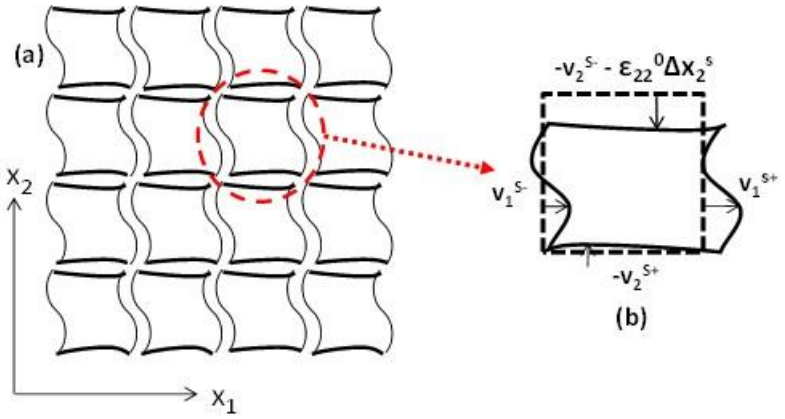

Figure 3.6. Schematic representative element area (REA) under applied strain (ε_{22}^{0}) with periodic boundary conditions

Periodic boundary condition is implemented on the REA as nodal displacement constraints through a Python language program appended to the previously obtained (for Model-II, Figure 3.5) orphan mesh file containing the periodic microstructure information. A specific strain is applied on the REA and the analysis is implemented through ABAQUS™ solver. Thus this approach simulates a strain- (or displacement) controlled test scenario. To efficiently handle post-processing of the simulated individual element stresses, a homogenization module is developed to obtain effective area-averaged REA stresses/strains[Sun and Vaidya 1996]and the effective individual phase stresses/strains. Figure 3.7(a) shows the generated periodic microstructure and Figure 3.7(b) shows the stress distribution obtained after analysis (Model-III) under the application of an imposed strain of 0.12% (which is well within the linear elastic range of cementitious systems). This value of strain provided an average REA stress of 36.13 MPa, which is very similar to the average REA stresses obtained for Models I and II when an external stress of 40 MPa was applied. Application of periodic boundary conditions on an REA under a strain-controlled regime eliminates all the boundary effects encountered in Models I and II. Hence this

model (Model III) is used for further analysis in this paper. Free quad-dominated 4-noded bilinear plane strain quadrilateral elements (CPE4R element implemented in ABAQUS^{TM}) are used in the FE models. A mesh convergence study was conducted so as to establish the mesh size for FE analysis. For an REA of 4.15 mm x 4.15 mm, a seed size of 0.0175 mm was found to yield converging responses for all sizes and volume fractions of inclusions. The finest mesh (68879 nodes and 68771 elements) that yielded a converged solution is shown in Figure 3.7(b) and is used in further simulations. The analysis scheme presented here does not consider the separation effects of phases (debonding) under stress. Application of low strains (or stresses) ensures adherence to the principles of linear elasticity and that the interface debonding effects are not dominant.

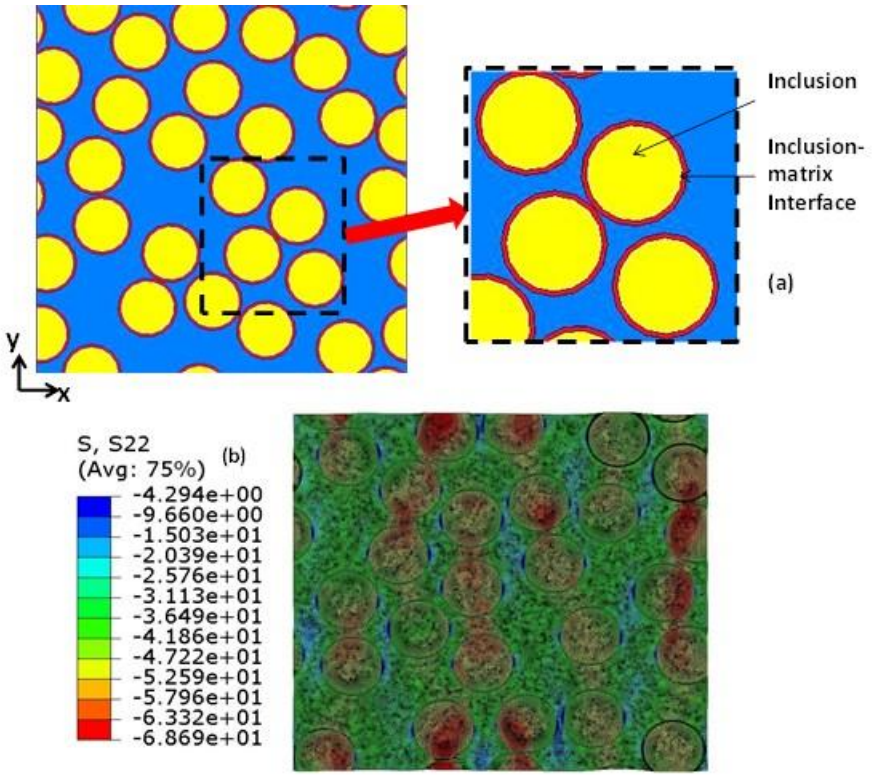

Figure 3.7. Model-III: (a) FE model showing the inclusions with the interfacial zones around them. The model contains 50% of inclusions by volume (or area); (b) effect of random distribution and periodic boundary conditions on the stress distribution under an imposed strain of 0.12%. The average REA stress is 36.13 MPa.

A flowchart that depicts the modeling and analysis sequence employed in this study is shown schematically in Figure 3.8. Area-averaged dominant principal stresses and strains in the REA, computed using the FE analysis, are calculated at different externally applied uniaxial displacements in order to obtain the effective composite Young's modulus.

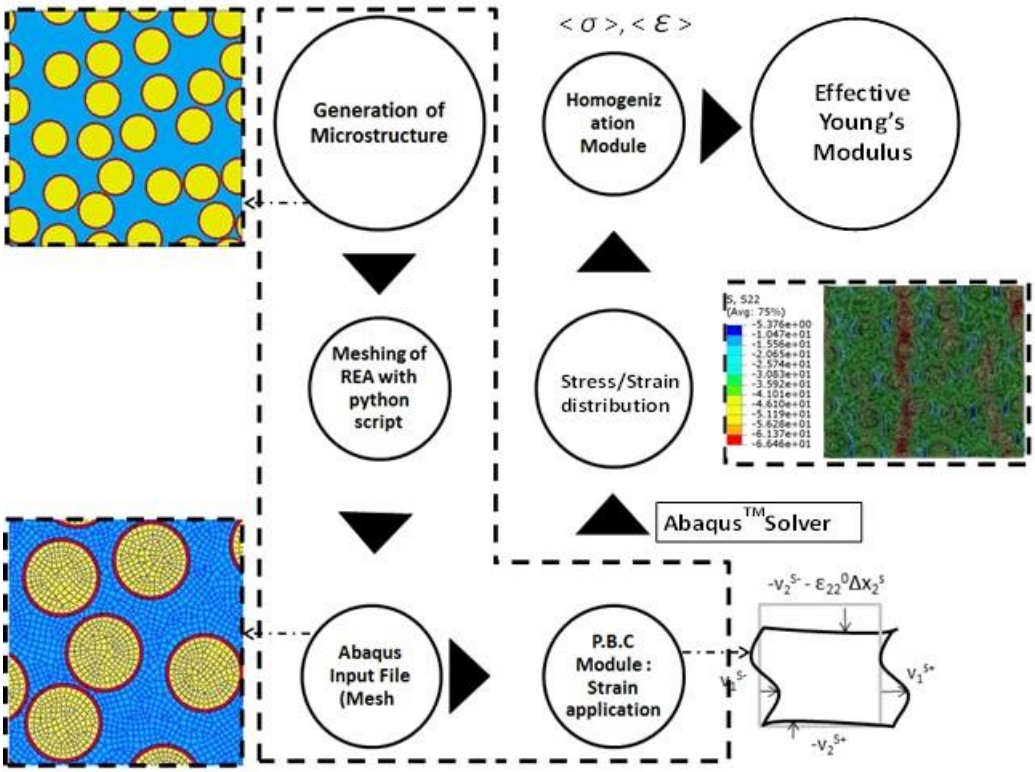

Figure 3.8. The sequence followed in the numerical analysis process including microstructural generation, meshing, application of periodic boundary conditions, homogenization, and determination of average REA stresses and effective E. (P.B.C denotes periodic boundary conditions).

Chapter 4: Influence of Inclusion Modification on Microstructural Stress Distribution and Linear Elastic Constitutive Response of Cementitious Mortar

Based on the discussions in the previous section, simulations are carried out on periodic virtual microstructures on which periodic boundary conditions are imposed (Model III). This section evaluates the sensitivity of the averaged (within a given phase or the REA) linear elastic stress responses as a function of varying material and geometric parameters of the microstructure, and brings out the fundamental differences in elastic response between systems containing hard (quartz) or soft (lightweight aggregates) inclusion particles. The size of inclusions is considered to be identical (600 μm) for both the quartz and lightweight aggregate systems, for simplicity. The default volume fraction of inclusions is 50%. However, the modeling technique and discussions presented herein are not restricted to such simplified systems and can tackle any realistic inclusion sizes and volume fractions. The effect of multiple inclusion sizes on the effective stresses is also demonstrated later in this thesis. The thickness of inclusion-matrix interface has been kept constant at 30μm for the simulations[Grondin and Matallah 2014; C. C. Yang 1998; Zanjani Zadeh and Bobko 2014]. The default material properties of different components are reported in Table 4.1.

4.1 Influence of Material Properties

In this section, the sensitivity of effective REA and individual phase stresses in quartz and LWA mortar systems to variations in material properties are evaluated. The constitutive relationships for all the components: cement paste, hard (quartz aggregates) and soft (lightweight aggregate - LWA) inclusions, and the paste-inclusion interfaces are considered in their respective linear elastic regimes only. The default elastic properties of

the components, extracted from available literature[Grondin and Matallah 2014; Z. Hashin and Monteiro 2002b; Ke et al. 2009; Lutz, Monteiro, and Zimmerman 1997; Nilsen, Monteiro, and Gjørv 1995; C. C. Yang 1998; Zanjani Zadeh and Bobko 2014], are presented in Table 4.1.However, for parametric studies discussed later in the paper, a range of values are considered, which are indicated in the respective sections.

Table 4.1. Elastic properties of the components of the mortar for FE simulations

Elastic property	Hardened cement paste	Quartz inclusion	Quartz-cement paste interface	LWA inclusion	LWA-cement paste Interface
Young's Modulus, E(GPa)	20	70	15	16	30
Poisson's Ratio, υ (--)	0.22	0.17	0.22	0.20	0.20

4.1.1 Influence of inclusion stiffness and prediction of composite E

Figures 4.1(a) and (b) show the dominant principal stress (σ_{22}) distribution considering the material properties shown in Table 1 for both the quartz and LWA mortar systems respectively, when a strain of 0.12% is applied to the REA. The LWA inclusions exhibit significantly higher deformation as compared to the quartz inclusions as can be seen from these figures, which is expected. While the quartz particles are highly stressed in the quartz mortar system, in the LWA mortar, it is the ITZ that bears the highest stress. This is expected considering the significantly higher stiffness of quartz particles as compared to that of LWA as shown in Table 4.1. Another distinct observation from Figure 4.1 is that the magnitude of stress inside the quartz particles increases when the particles are very close to each other, attributable to the significant stiffness mismatch between the inclusions and the matrix. On the contrary, LWA mortar does not exhibit an increase in

stress inside LWA. Instead, the stress concentration in the ITZ is higher if the neighboring particles are close to each other. Thus, the relative stiffness of the inclusions with respect to the matrix results in distinctively different stress distributions, and thus differing propensities of failure in the microstructure. Note that the magnitude of the maximum dominant principal stresses (σ_{22}), which occur in the inclusions when the inclusion is stiffer and the inclusion-paste stiffness mismatch is higher, and in the ITZ when inclusion-paste stiffness mismatch is lower, are rather comparable. The quantified averaged REA stress and the stresses in the other microstructural phases are plotted in Figure 4.2 as a function of the inclusion stiffness.

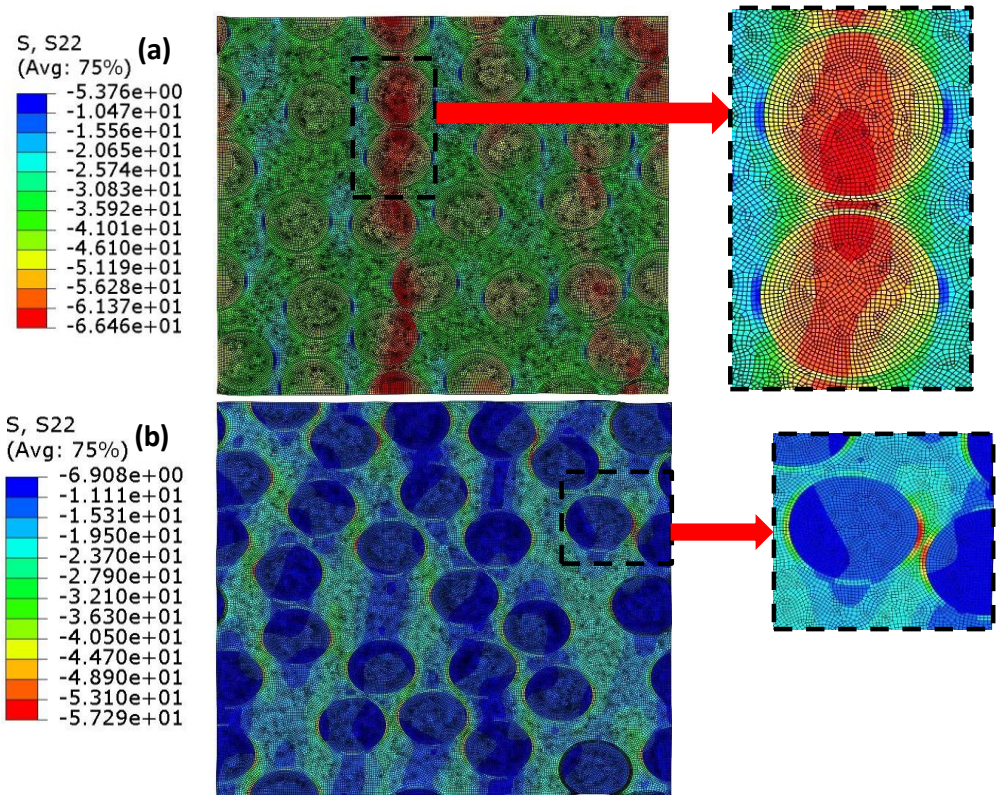

Figure 4.1. Dominant principal stress (σ_{22}) (MPa) distributions in: (a) quartz mortar system and (b) lightweight aggregate mortar system. Magnified representation of stress distributions in both mortar systems containing the zones around the inclusions are shown for clarity. The REA is subjected to a strain of 0.12%.

Figure 4.2(a) shows the area-averaged dominant principal stresses in the REA as well as those in the individual microstructural phases for a mortar system containing quartz particles as a function of the Young's modulus of quartz (in the range of 50 to 100 GPa). With increasing E of quartz (at the same inclusion volume fraction, and leaving the E of the paste and the interface unchanged), the average stresses in all the phases in the microstructure increase linearly. The quartz inclusions experience the highest average stress amongst all the phases because of the significantly higher E values compared to the paste or the ITZ, in line with Figure 4.1(a). The ITZ and the paste matrix components show similar averaged stresses, attributable to the fact that the stiffness difference between these phases is negligible when compared to the difference in stiffness between quartz and these phases. Figure 4.2(b) shows the averaged REA and other component stresses in the LWA mortar system for varying stiffness of LWA inclusions (between 6 and 21 GPa[Ke et al. 2009]). Here, the highest stress is observed in the ITZ as shown in Figure 4.2(b) because of the fact that its stiffness is the highest among all the phases in this microstructure. While the average stress increases in all the phases when stiffer LWA is used, the rate of increase in stress is higher in the LWA inclusions compared to the other phases or the REA. The average stress in the cement paste matrix and ITZ of the LWA mortar system linearly increases with LWA stiffness whereas the stress increase in the LWA inclusions is found to be nonlinear, primarily attributed to the deformational effects of the LWA and the consideration of perfect bonding between the phases in the model. The rate of stress increase in the LWA and the paste decreases with increasing LWA stiffness and the stresses in these phases are almost equal when the LWA and the paste stiffness are similar, as expected. Figures 4.2(a) and (b) also show that the averaged stresses in all the components

are lower in the LWA system as compared to those in quartz mortar system. This can be attributed to the stresses concentrated over large areas in quartz particles that increases the average inclusion stresses as well as the other phase stresses in quartz mortar system due to assumption of perfect bonding between phases. On the contrary, LWA system shows lower stresses due to lower stiffness of LWA inclusions as well as lower effective stiffness of REA. Furthermore, several important, microstructure-based design-relevant considerations are obtained through these simulations, which are summarized below:

(i) Although significant stress concentrations are observed inside stiff particles in the quartz mortar, the interfaces between the paste and the inclusions are more critical since ITZ is the weakest component in this system and the stiff inclusions can sustain significantly higher load without failure. The average stress in ITZ increases by about 16% and the average REA stresses by about 20% when the E of the stiff inclusion is doubled, denoting that there is no significant advantage in terms of propensity to fail (strength) even if a very stiff (and thus generally strong) inclusion is used, unless the paste (and interface) properties are concurrently altered. However, at low strains, the beneficial effects of a higher composite stiffness also cannot be discounted;

(ii) Even though the inclusions in the LWA mortar exhibit the lowest stress among all the components under applied external strains, the softer and weaker (compared to the cement paste matrix and ITZ) LWA inclusions are critical towards failure of LWA mortar system;

(iii) Tripling the stiffness of LWA inclusions (within limits without compromising various benefits of LWAs such as low density and thermal performance) results in more than doubling of the stress in the LWA inclusions. While stiffening of LWA inclusions

increases the stress inside LWA inclusions, the strength of the inclusions also likely increases concurrently. Hence a suitable combination of stiffening and strengthening of LWA inclusions can be selected for optimal mechanical performance;

(iv) Increase in stiffness of LWA inclusions is also associated with increase in stress in the ITZ and matrix. Hence, the results indicate that the ITZ and matrix also needs to be strengthened if the LWA stiffness (and strength) is to be increased. These results exhibit that the fundamental material-design approach, which is based on traditional stiff inclusion incorporation, needs to be altered when softer inclusions are incorporated in cementitious systems.

The modeling approach and the results described here indicate the probable failure modes and provide valuable information on the mechanical performance and design of particulate composite materials such as mortars and concrete, especially when new inclusion materials are used for specific performance features or to address sustainability issues (e.g., the use of different types of soft inclusions such as LWAs for internal curing [Bentz and Snyder 1999; Cusson and Hoogeveen 2008], fly ash-based aggregates [Kayali 2008; Wasserman and Bentur 1997], microencapsulated phase change materials for thermal cracking control [Fernandes et al. 2014], and waste and recycled materials such as rubber for energy absorption[Hernández-Olivares et al. 2002]).It is reiterated that the models consider perfect bonding between the particles and the matrix; a case not completely realistic, but helps provide comparisons of material response.

Figure 4.2(c) shows the constitutive response of the quartz and LWA mortars containing 50% of inclusions by volume, extracted from numerical simulations. The dominant principal stresses (σ_{22}) and principal strains (ε_{22}) in the linear elastic range of

these systems are used. Thus the approach presented here can be used to determine the composite elastic moduli of systems containing multiple inclusion types. In addition to the E value, as described earlier, this methodology also provides estimates of the microstresses in the different phases under imposed strains (in the linear elastic regime) and facilitates the development of constitutive relationships for composite materials, which otherwise would be experimentally tedious. Comparison of Young's modulus values obtained from numerical simulation (FEA) to those calculated using analytical/semi-analytical approaches as well as experimental validation of the adopted numerical technique is detailed in a later section of this paper.

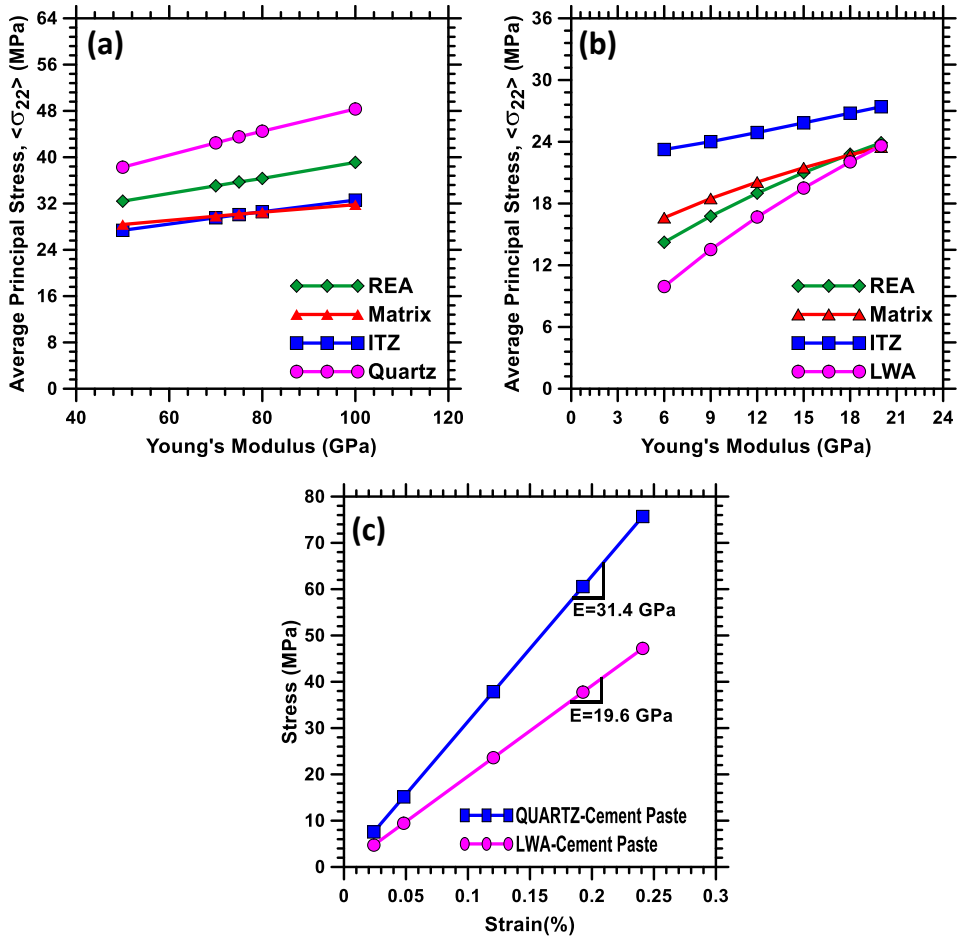

Figure 4.2. Effective REA and individual component stresses (σ_{22})as a function of inclusion stiffness for: (a) quartz mortar system and (b) LWA mortar system; and (c) linear constitutive relationship for quartz and LWA mortar systems for defaults values of material parameters (shown in Table 4.1) and microstructural features.

4.1.2 Influence of ITZ stiffness

Figure 4.3(a)shows the area-averaged dominant principal stresses in the REA as well as those in the individual microstructural phases for a mortar system containing quartz particles as a function of the Young's modulus of ITZ (in the range of 8 to 18 GPa). With increasing E of the ITZ (at the same inclusion volume fraction, and leaving the E of the paste and the quartz inclusion unchanged), the average stresses in all the phases in the microstructure increases. The rate of increase in the stresses is highest in the ITZ which is

to be expected as the ITZ is being stiffened. The stresses in the matrix and the quartz inclusion are still higher than that of the ITZ, which is attributed to their higher stiffness compared to that of the ITZ. For a E of ITZ close to that of the matrix, it is observed that the stresses in the ITZ are almost similar to that in the matrix. This is significant as the ITZ is the weakest component in the quartz mortar system and is the region where failure is most likely to first occur. With a stiffer ITZ, failure would be most likely be delayed as the strength of the ITZ would also increase, thereby enabling the REA to take more load than with a softer ITZ. Figure 4.3(b) shows the area-averaged dominant principal stresses in the REA as well as those in the individual microstructural phases for a mortar system containing LWA particles as a function of the Young's modulus of ITZ (in the range of 20 to 40 GPa). In the case of the LWA mortar system, the ITZ is the stiffest component of the composite microstructure. As such, the stresses are highest in the ITZ compared to the matrix and the LWA inclusion. Another observation from figure 4.3 b is that the stresses in the matrix and the LWA inclusion do not show much change with increasing ITZ stiffness. This is due to the fact that even though the ITZ is stiffer than both the matrix and the inclusion, the difference in the stiffness between the phases is not large.

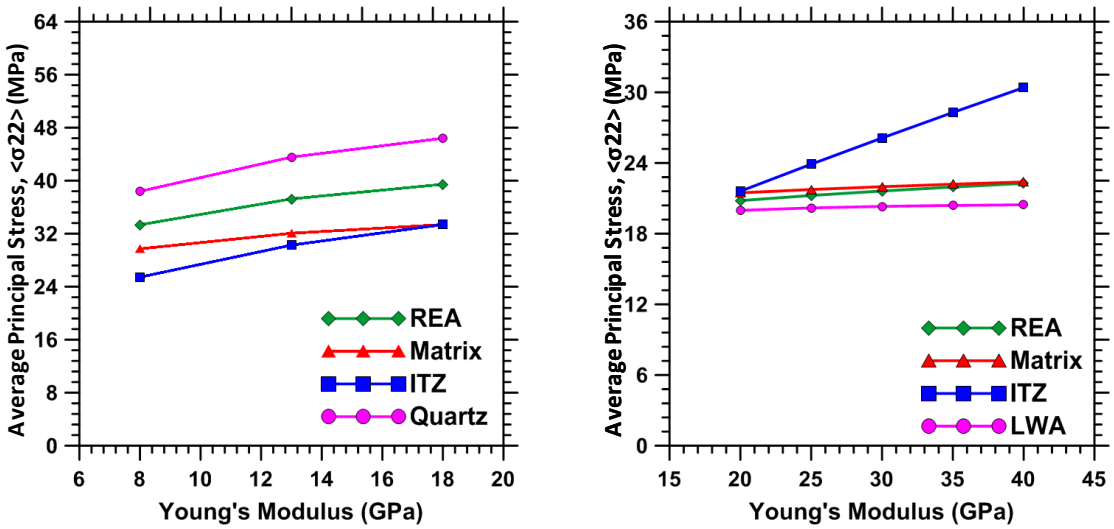

Figure 4.3. Effective REA and individual component stresses (σ_{22}) as a function of ITZ stiffness for: (a) quartz mortar system and (b) LWA mortar system.

4.1.3 Influence of ITZ thickness

Figure 4.4(a)shows the area-averaged dominant principal stresses in the REA as well as those in the individual microstructural phases for a mortar system containing quartz particles as a function of the thickness of ITZ (in the range of 20 to 50μm). With increasing thickness of the ITZ (at the same inclusion volume fraction, and leaving the E of the paste, ITZ and the quartz inclusion unchanged), the average stresses in all the phases in the microstructure decreases. With an increase in the thickness of the ITZ, the area of low stiffness around the inclusion increases and as such, stress transfer into the inclusion is impeded. This is reflected in the drop in the stresses in the quartz inclusion phase with increasing thickness of the ITZ. This is not a desirable condition, as it defeats the purpose of using a stiff inclusion. With increasing thickness, the stresses in the ITZ decrease but the drop is not significant enough to warrant that failure would be delayed or would not occur. Figure 4.4(b) shows the area-averaged dominant principal stresses in the REA as well as those in the individual microstructural phases for a mortar system containing LWA

particles as a function of the thickness of ITZ (in the range of 10 to 50μm). With increasing thickness of the ITZ (at the same inclusion volume fraction, and leaving the E of the paste, ITZ and the quartz inclusion unchanged), the average stresses in all the phases in the microstructure do not show any significant change. With an increase in the thickness of the ITZ, the area of stiffer region around the inclusion increases and as such, stresses should concentrate on the ITZ, but the overall volume fraction of the ITZ in the microstructure is not large enough to cause any deviation in the stresses with an increase in its thickness. The stresses in the LWA inclusion also do not show much change and as such would be still critical towards failure of LWA mortar system. From figure 4.4 it is evident that increase in the thickness of ITZ does not have much beneficial effect on the stresses both in the individual components and the REA in the quartz and LWA mortar systems.

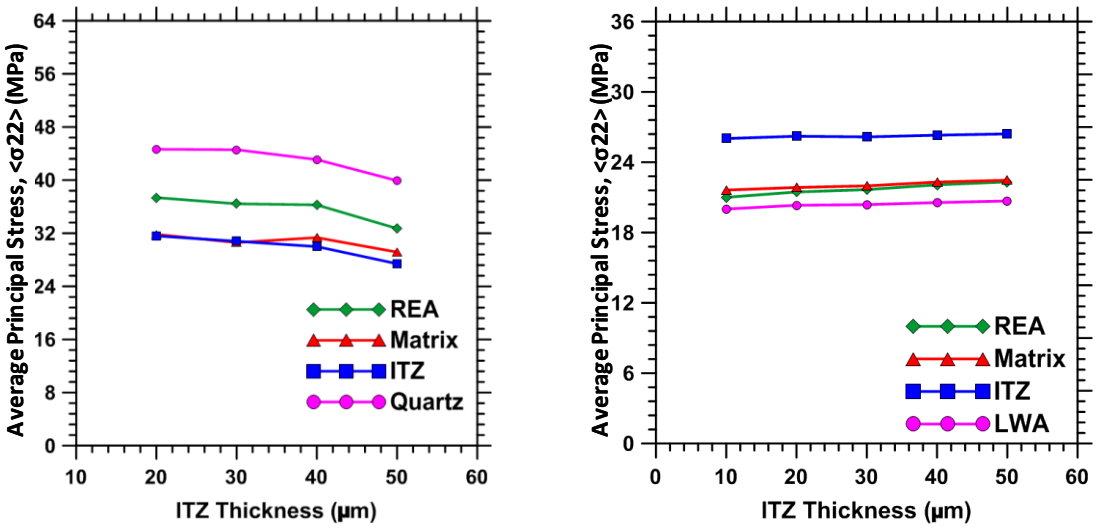

Figure 4.4. Effective REA and individual component stresses (σ_{22}) as a function of ITZ thickness for: (a) quartz mortar system and (b) LWA mortar system.

4.1.4 Influence of matrix and ITZ stiffening

This section reports the influence of matrix as well as ITZ strengthening/stiffening (such as those accomplished through the use of additives like silica fume as a partial replacement of cement) in mortars containing quartz or LWA as inclusions with an aim of understanding the relative influences of matrix modification. The Young's modulus of silica fume modified cement paste is taken as 25 GPa[C. Hu and Li 2015] as opposed to 20 GPa for the unmodified systems. The stiffness of the ITZ was also increased proportionally (Young's modulus of ITZ is taken as 18.75 and 37.5 GPa in quartz and LWA mortars respectively) since silica fume incorporation is known to result in interface densification and stiffening [Duan et al. 2013; C. Hu and Li 2015]. Figures 4.5(a) and (b) show average stresses in the REA as well as in the individual microstructural phases corresponding to an applied strain of 0.12% for the quartz and LWA mortars respectively. Stresses increase in all the phases for both the mortar types when the paste phase contains silica fume. In the quartz mortar, the average stress in the ITZ increased by about 15% when 10% silica fume was incorporated. However, the strength enhancement of both the ITZ and the paste phase will likely be larger than the stress increase, thereby rendering improved mechanical performance to the quartz mortar when silica fume is incorporated in the paste phase. This has been demonstrated through experimental studies [C. Hu and Li 2015; Shannag 2000]. The stress increase inside the quartz inclusions has an insignificant influence on material failure because of the higher strength of quartz particles [Axelson and Piret 1950]. On the contrary, the inclusions in the LWA mortar system are relatively weak and even a marginal increase in inclusion stress is likely to result in material failure at even lower applied strains as compared to that in LWA mortar systems without silica

fume incorporation. Thus the combined stiffening of ITZ as well as the matrix in LWA mortar system has a detrimental effect on the strength, provided it is the lightweight inclusion that is weaker and fails first. This points to the fact that matrix strengthening methods such as the use of silica fume might not be beneficial from a viewpoint of mechanical response in these systems, unless the LWA is stronger. However, the densification of the matrix and the ITZ will still lead to better durability properties in such concretes.

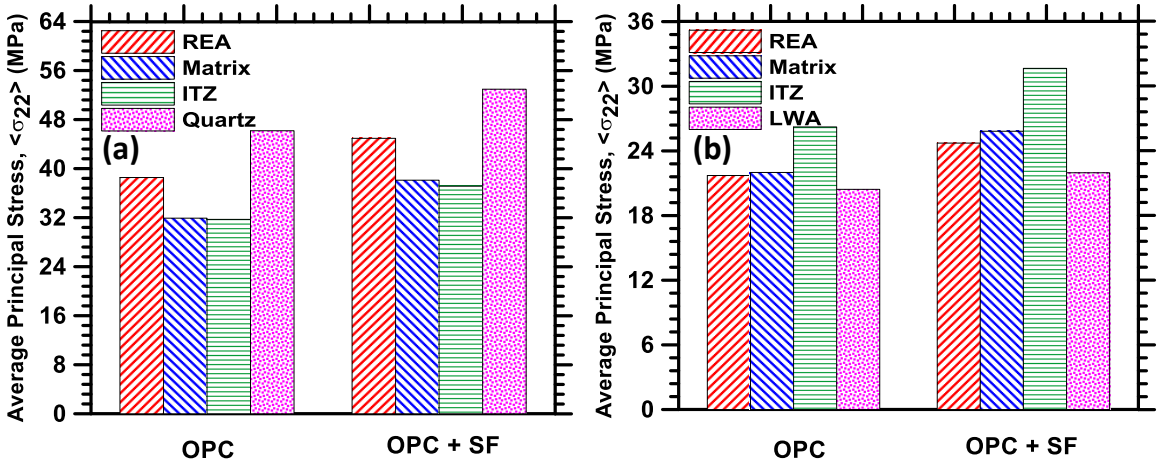

Figure 4.5. Effect of silica fume incorporation on the average REA and phase stresses for: (a) mortar containing quartz inclusion, and (b) mortar with LWA inclusions. The modified matrices contain 10% silica fume by mass as a cement replacement material.

4.2 Influence of Inclusion Content

The preceding sections have dealt with systems containing a constant inclusion volume fraction of 50%. Figures 4.6(a) and (b) show the effect of inclusion volume fraction on the average principal stresses in the quartz and LWA mortars respectively. With increasing volume fraction of inclusions, the average REA stresses as well as the stresses in all the phases in both the systems increase linearly. For the quartz mortar (Figure 4.6(a)), the rates of stress increase in the microstructural phases as well as the REA as a function

of the inclusion volume fraction are higher as compared to those in LWA mortar (Figure 4.6(b)). This is once again attributed to the higher stiffness of quartz inclusions. While an increase in the ITZ stress at higher volume fractions of quartz is likely to be responsible for interface failure (since ITZ is the weakest component in the quartz mortar) and thus the material failure under smaller applied strains in quartz mortar, a stress increase inside the LWA inclusions (which is the weakest component in the LWA mortar) at higher volume fractions of LWA is expected to be the cause of failure of LWA mortar system under smaller external applied strains.

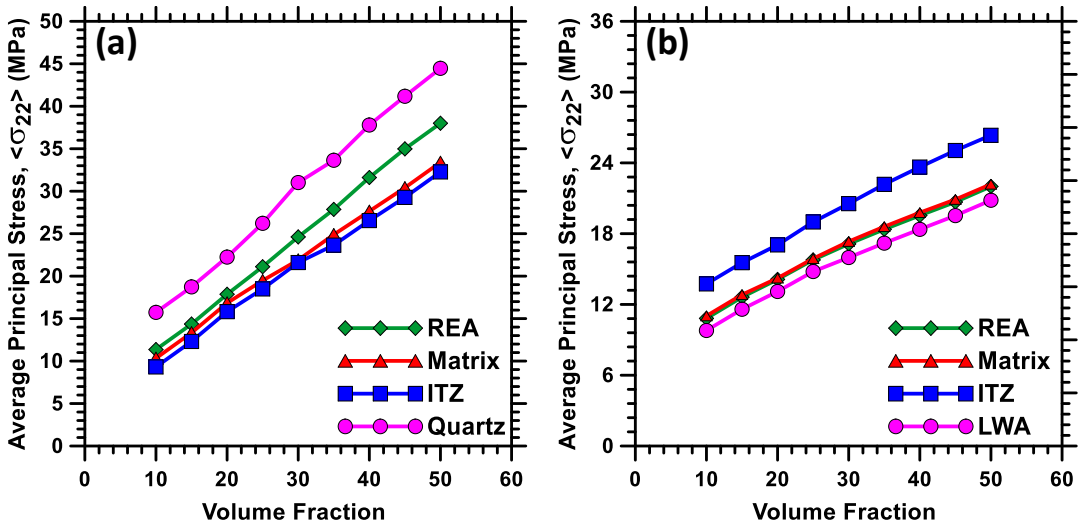

Figure 4.6. Effective REA and individual phase stresses as a function of inclusion volume fraction for: (a) quartz mortar and (b) LWA mortar.

4.3 LWA Mortar with Multi-Sized Particles: Microstress Distribution and REA Stresses

While all the previous parametric studies considered the response of systems with single sized inclusions, the influence of several inclusion sizes (as is the realistic case) on the average REA and phase stresses is dealt with in this section. Default values of

material/geometrical properties of inclusions, paste, and ITZ (Table 4.1) are used here. Table 4.2 shows the three different uniform inclusion size distributions used in this study. The inclusion sizes are uniformly distributed around a mean of 0.6 mm and standard deviations of 0.06, 0.12, and 0.24 mm respectively. Figures 4.7(a) and (b) show the dominant principal stress (σ_{22}) distribution in single- and multi-sized particulate (LWA) systems respectively. Here, LWA inclusions with a mean size of 0.6 mm and a standard deviation of 0.24 mm are considered. Figures 4.7(a) and (b) also show enhanced stress concentrations between the closely spaced inclusions, especially if they are aligned in a direction perpendicular to that of the applied strain. In Figure 4.7(b), when smaller particles, particularly with varying sizes are in proximity with each other, a slight stress relaxation trend is observed. With smaller particles, there is a reduction in the continuous volume of ITZs (the highly stressed phases in the LWA mortar systems) that are adjacent to each other, resulting in such an observation. These are reflected in the individual phase stresses as well as the average principal REA stresses for the different particle size distributions, which are shown in Figures 4.8(a) and (b) respectively. These figures provide average stress information on mortars containing 50% LWA inclusions by volume. The averaged stresses are highest in the single-sized LWA mortar due to the higher stress concentrations in the inter-inclusion areas as explainer earlier. The stresses reduced considerably (by about 20%) when non-uniform particle sizes are considered since interactions between neighboring smaller and larger particles reduce the stresses, contrary to the higher stress-concentrations encountered between two closely spaced similar-sized inclusions. For the same reason, the averaged REA stresses also decrease as the inclusion

size distribution is more spread out (the mean size being the same), as reflected in Figures 4.8 (a) and (b).

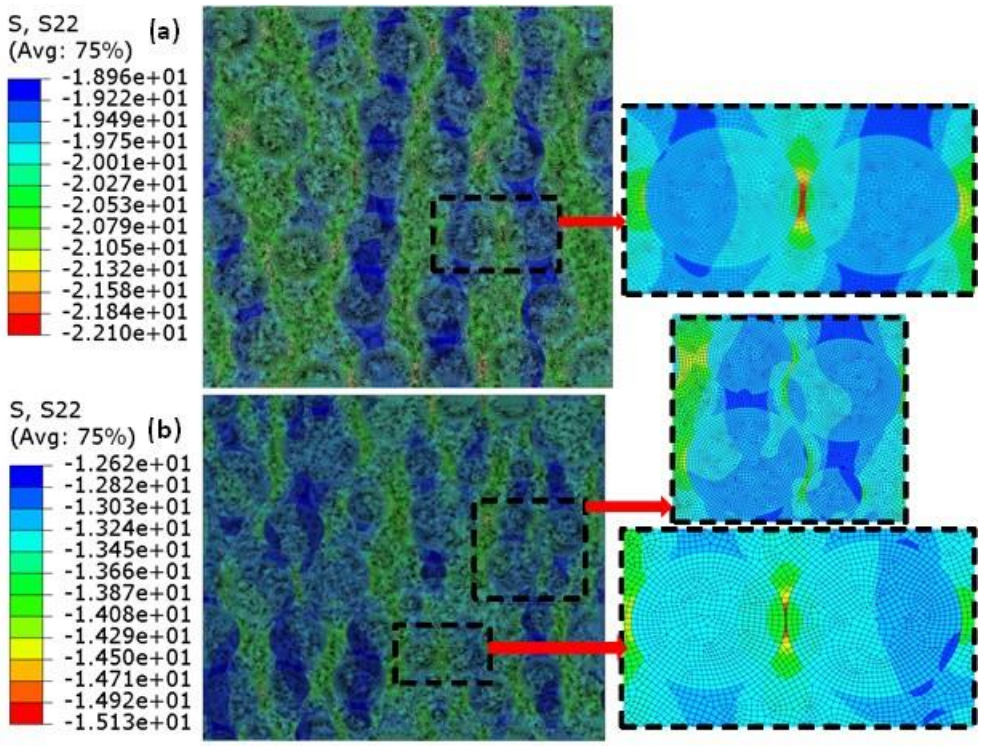

Figure 4.7. Influence of particle sizes on the dominant principal Stresses (MPa) in the REA for: (a) single-sized LWA inclusions, and (b) multiple sized (Mean = 0.6 mm and std. dev. = 0.24 mm) LWA inclusions embedded in a cement paste. Magnified representation of stress distributions in the vicinity of the particles (similar and dissimilar sizes) are shown for clarity.

Table 4.2. Size distributions (uniform distribution) of the LWA particulate inclusions for FE simulation

PSD Type	Range (mm)	Mean (mm)	Std. Dev. (mm)
Single Size	NA	0.6	0
Multiple Size (Narrow)	0.5-0.7	0.6	0.06
Multiple Size (Medium)	0.4-0.8	0.6	0.12
Multiple Size (Wide)	0.2-1.0	0.6	0.24

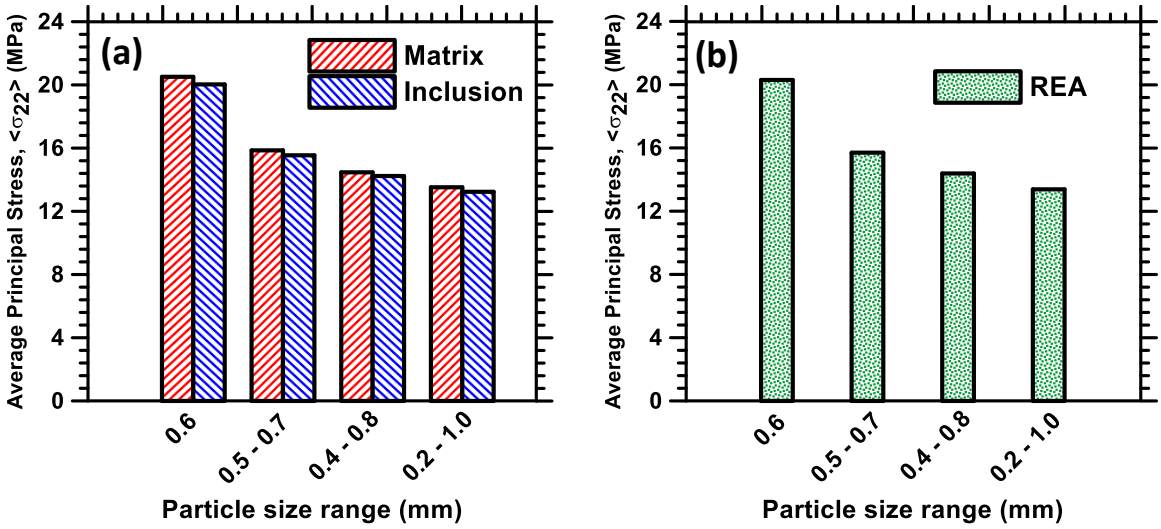

Figure 4.8. Effect of LWA inclusion size distribution on: (a) the matrix and inclusion stresses; and (b) effective REA stresses (mean particle size is 0.6 mm)

4.4 Micromechanics-Based Elastic Modulus Predictions

4.4.1 Comparison with analytical modeling schemes

Predicting the material properties of composite systems is an important attribute desired from a micromechanical model, so that material design decisions could be made in a rational manner with limited experiments. This section compares the composite Young's modulus values predicted using the above-described micromechanical model as well as using well-established analytical models such as Mori-Tanaka[Mori and Tanaka 1973b], double inclusion [Hori and Nemat-Nasser 1993] and Hobbs method[Hobbs 1971].Mori-Tanaka (M-T) method has been previously used for determination of effective properties of cement-based materials[da Silva, Němeček, and Štemberk 2013; G. K. Hu and Weng 2000; Miled, Sab, and Le Roy 2011; C. C. Yang 1997]. It considers a discrete spherical inclusion embedded in an infinitely extended homogeneous reference medium (matrix). The homogenized elastic moduli for two-phase materials can be quantified from the individual phase properties as recently explained in [Das et al. 2015; Mori and Tanaka

1973b]. A two-step homogenization is performed for the determination of effective Young's modulus for binder systems using the M-T method. In Step I, the cement paste and ITZ are homogenized and in Step II, the inclusions and the resultant phase from Step-I (which is the new reference medium) are homogenized. While the Mori-Tanaka model consists of an ellipsoidal inclusion in an infinitely extended homogeneous reference medium, the double inclusion (DI) model considers an ellipsoidal inclusion embedded in another ellipsoidal matrix, which is further embedded in an infinitely extended homogeneous medium [Hori and Nemat-Nasser 1993; C. C. Yang and Huang 1996a]. Detailed derivation and analysis procedure are described in [Hori and Nemat-Nasser 1993; G. K. Hu and Weng 2000; C. C. Yang and Huang 1996a]. Here the inclusion (quartz or LWA) is considered to be embedded in ITZ, and this composite particle is embedded in an infinite cement paste matrix.

Another analytical homogenization approach derived by Hobbs [Hobbs 1971]is also used here for comparison. The resultant homogenized Young's modulus (E*) for a two-phase composite is given as:

$$E^* = E_m \left[1 + \frac{2\phi_i(E_i - E_m)}{(E_i + E_m) - \phi_i(E_i - E_m)}\right] \tag{4.1}$$

where ϕ_i is the volume fraction of the inclusions, and E_i and E_m are the Young's modulus of the inclusion and matrix respectively. Here also, a two-step homogenization procedure for the multiple phases as adopted for the M-T method is carried out in order to obtain the homogenized Young's modulus.

While the analytical models can predict only the elastic modulus of the composite, the micromechanical model presented in this paper also provides the average linear elastic

stresses and strains in the REA (in addition to the stresses in the different microstructural phases) from which the effective Young's modulus can be determined. Figures 4.9(a) and (b) show the composite Young's modulus with varying inclusion volume fractions for quartz and LWA mortar systems respectively. The Young's modulus increases significantly in the quartz mortar with increasing volume fraction of inclusions whereas it decreases with increasing inclusion volume fraction in the LWA mortars, as expected. In both the systems, the M-T and double inclusion models predict higher values of Young's modulus as compared to those quantified using the micromechanical FE analysis. This is because these analytical schemes do not adequately capture the realistic inter-inclusion interactions that result in stress-concentrations/relaxations in these micro-heterogeneous systems that influence the composite REA stresses for a given imposed strain. Hobbs method is also a simple geometry-independent and volume-fraction based analytical method which also does not capture stress-concentrations in heterogeneous systems with complex geometries. On the contrary, a numerical scheme such as the one described here adequately captures such interactions[Dunant et al. 2013].Besides, the accuracy of the analytical homogenization techniques has been shown to be limited if the stiffness contrast between the phases is high [Dunant et al. 2013; Idiart et al. 2009].This is reflected in Figures 4.9(a) and (b) that shows the predicted elastic modulus as a function of the inclusion volume fraction for both the quartz and LWA mortars. In the quartz mortar system ($E_{inclusion}/E_{paste}$= 3.5) with 50% inclusion volume fraction, the analytical schemes (M-T and DI) predict about 20% higher value of homogenized Young's modulus as compared to the micromechanical FE analysis. On the other hand, the homogenized Young's moduli predicted using analytical schemes are about 10% higher than that

quantified using the FE analysis for the LWA mortar system ($E_{inclusion}/E_{paste}$= 0.8).In the case of quartz mortar, the Young's modulus predicted by Hobbs method correlates well with that obtained using numerical simulation at lower quartz volume fractions (up to 30%). However, the predictions diverge at higher quartz volume fractions because of the dilute limit being exceeded and the inter-particle interactions becoming dominant, the effect of which cannot be accounted for by analytical models. The trends in Figure 4.9 suggest that Hobbs method over-predicts the Young's modulus as compared to numerical approach when the inclusions are stiffer than the matrix and under-predicts it when the inclusions are softer than the matrix. A comparison of the results from the numerical analysis scheme to the experimentally determined elastic moduli is shown in the forthcoming section.

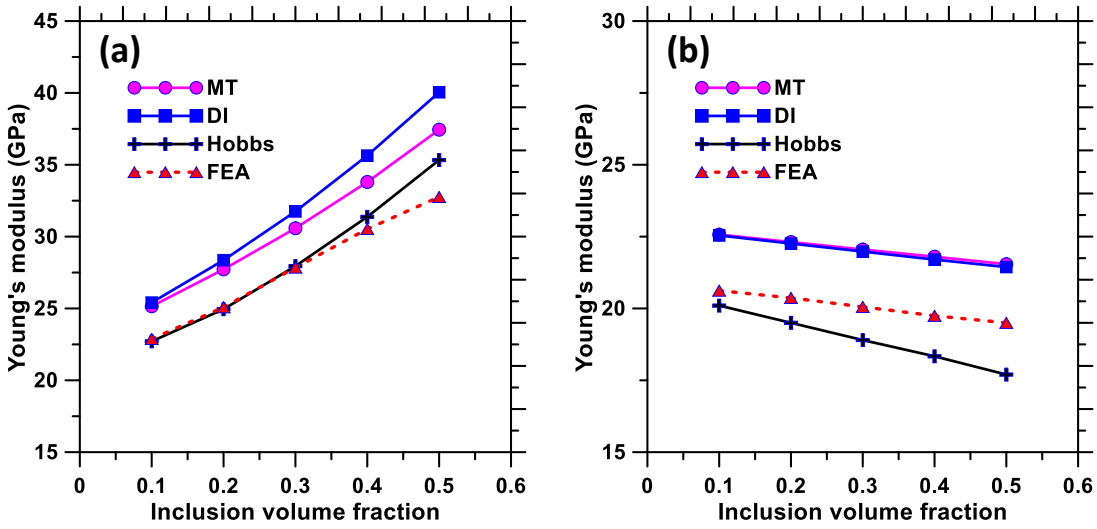

Figure 4.9. Young's modulus predicted using the micromechanical model and its comparison with well-established analytical models for: (a) quartz mortar and (b) LWA mortar

4.4.2 Experimental validation

To validate the micromechanical FE model, experimental values of Young's modulus of quartz mortar at different volume fractions of quartz has been adopted from an experimental study [Falzone et al. 2015] where the elastic modulus was measured in accordance with ASTM C469, using cylindrical specimens (10cm diameter x 20cm height). For numerical simulations, the Young's modulus of quartz, cement paste and ITZ were taken as 64 GPa, 16.75 GPa and 8.375 GPa respectively, ITZ thickness as 5 μm, and the Poisson's ratio of all the components as 0.22as reported in the above-referenced experimental study. Four different volume fractions of quartz (10, 20, 30 and 55%) are used for simulations. For the numerical analysis, four replicate microstructures with random spatial distributions were generated for each of the inclusion volume fractions. The median inclusion size of quartz for the micromechanical analysis was matched to those used in the experimental studies (365 μm). Figure 4.10 shows the Young's modulus of quartz mortar, predicted using the FE scheme (principal stresses and strains measured in the REA, when the microstructure was subjected to different strains in the linear elastic regime, as shown in section 4.1.1) along with the experimental measurements. A very good correlation is noticed between the predicted and measured Young's modulus as can be seen from this figure, contrary to the analytical schemes described earlier, establishing the viability of using the numerical homogenization scheme in determining the Young's modulus of micro-heterogeneous systems. Also, the standard deviations of the predicted Young's modulus values from four replicate microstructures are negligible as compared to standard deviations of experimental measurements, reinforcing the efficacy of using microstructure-guided numerical simulation towards prediction of Young's modulus.

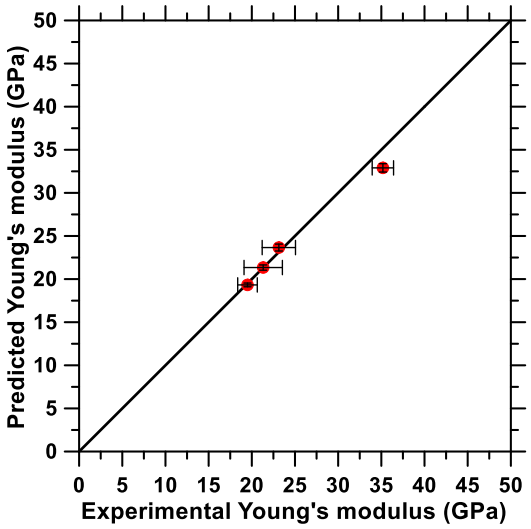

Figure 4.10. Relationship between experimentally obtained E value and those predicted using the micromechanical FE scheme for a mortar containing different volume fractions of quartz particles.

Chapter 5: Influence of Interfacial Debonding on the Microstructural Stress Distribution and Linear Elastic Constitutive Response of Cementitious Mortar

Interfacial debonding is one of the prime factors which influence the macroscopic constitutive response of a particle reinforced composites. The current chapter presents a framework capable of capturing the influence of interfacial debonding on the finite deformation response of particle reinforced composites. The influence of debonding is accounted for through the use of traction-separation relationship. This chapter evaluates the sensitivity of the averaged REA linear elastic stress responses as a function of varying material and geometric parameters of the microstructure, and brings out the fundamental differences in elastic response between systems containing hard (quartz) or soft (lightweight aggregates) inclusion particles when interfacial debonding is considered. The mean size of inclusions is considered to be identical (600μm) with a variance of (400μm) and a standard deviation of (240μm) for both quartz and lightweight aggregates systems, for simplicity. The default volume fraction of inclusions is 30% so as to reduce the computational demand. The thickness of inclusion-matrix interface has been kept constant at 30μm for the simulations [Meier, Kuhl, and Steinmann 2008b; Wriggers and Moftah 2006a; M. Chi and Huang 2013]. The default material properties of different components of the composites are reported in Table 4.1.

5.1 Traction-Separation Law

The major challenge in the cohesive zone model is the determination of the traction–separation relationship. For plain concrete, a linear softening model was employed by [Hillerborg, Modéer, and Petersson 1976], and a bilinear softening model was introduced by [Petersson 1981]. Since then, a bilinear softening model has been widely

utilized [Bazant and Planas 1997]. The majority of cohesive zone models are based on intrinsic formulations which require a pre-defined debonding path and penalty stiffness prior to the softening behavior, as shown in Figure 5.1.a. The intrinsic CZM has four stages as shown in Figure 5.1.b. The first stage is characterized by general elastic material behavior without separation (Figure 5.1.b : Stage I).The quasi-brittle material properties are assumed to be homogeneous and linear elastic in this stage. The next stage is the initiation of debonding when a certain criterion is met, for example, critical tensile bending stress(Figure5.1.b: Stage II).In this study, the fracture initiation criterion for mode I fracture is assumed to occur when the state of stress reaches the cohesive strength (e.g. concrete tensile strength, f'_t).Stage III describes the evolution of the debonding, which is governed by the cohesive law or the softening curve, i.e., the relation between the stress (r) and crack opening width(w) across the debonded surface, as shown in Figure5.1.b (Stage III).

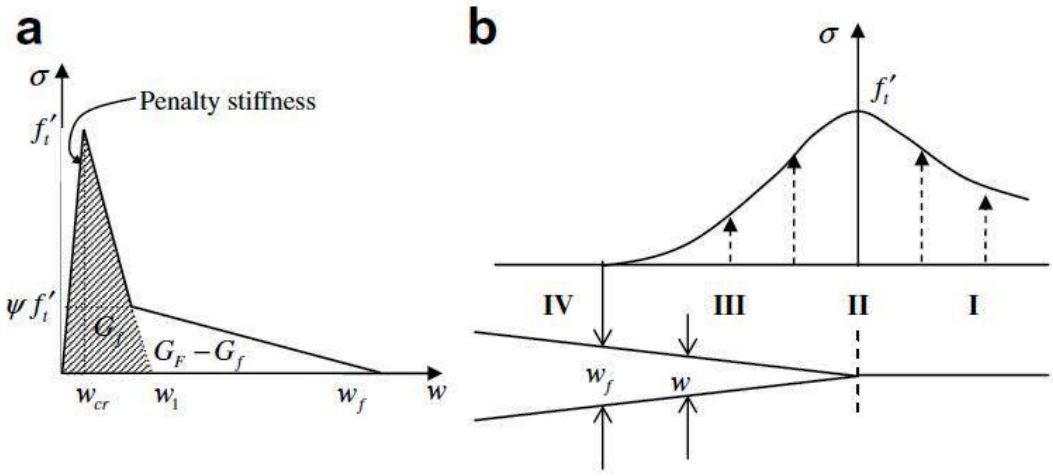

Figure 5.1 (a) Bilinear softening for quasi-brittle materials and (b) four stages of the cohesive zone model[Roesler et al. 2007]

Different constitutive relationships, such as a linear[Hillerborg, Modéer, and Petersson 1976], bilinear[Petersson 1981; Roelfstra and Wittmann 1986; Park, Paulino, and Roesler 2008], trilinear[Cho et al. 1984], and exponential [Gopalaratnam and Shah 1985] softening curve, have been developed to predict interfacial debonding. Among the various softening curves, the bilinear softening relationship has been used extensively and has been chosen in this work. [Petersson 1981] originally proposed a bilinear softening curve with a fixed kink point, which was also adopted by [Gustafsson and Hillerborg 1985].[Wittmann et al. 1988] determined a bilinear softening curve with the stress ratio of the kink point at 0.25.[Elices et al. 2002] and [Guinea, Planas, and Elices 1994] characterized a bilinear softening curve using the tensile strength, the total fracture energy, and two parameters which represent the shape of a softening curve.[Bažant 2002] further refined the bilinear softening model by introducing an additional fracture parameter called the initial fracture energy. In this research, the bilinear softening model [Bažant, Yu, and Zi 2002] was selected since the softening curve has two slopes which can be controlled by the measured fracture properties. The CZM has been mentioned above to describe the various stages and in particular the stage at which traction-separation relationship affects the softening curve. In this research, only the traction-separation relationship is used to account for debonding at the interfaces between the matrix and the inclusions. The following experimental fracture parameters that define the bilinear softening curve shape are simple to measure using Two Point Beam (TPB) and split tensile testing configuration: total fracture energy (G_F), initial fracture energy (G_f), and tensile strength (f'_t).

In order to evaluate the interfacial debonding, this research utilizes a bilinear softening model [Park, Paulino, and Roesler 2008]. The bilinear traction-separation model is defined by four experimental fracture parameters:

- tensile strength (f'_t)
- initial fracture energy (G_f)
- total fracture energy (G_F) and
- fracture toughness (K_{IC})

The values for the four experimental fracture parameters; the tensile strength (f'_t), initial fracture energy(G_f), total fracture energy(G_F) and fracture toughness(K_{IC}) which define the bilinear softening model for ordinary portland cement are adopted from the literature [Das et al. 2015; Das et al. 2016].

5.2 Influence of Interfacial Debonding on the Micro-Stress Distributions and Effective Young's Modulus

The approach presented here can be used to determine the composite elastic moduli of systems containing multiple inclusion types. In addition to the E value, as described earlier, this methodology also provides estimates of the microstresses in the different phases under imposed strains (in the linear elastic regime) and facilitates the development of constitutive relationships of composite materials while considering the effect of debonding. Figure 5.2 (a) and (b) show the constitutive response of the quartz and LWA mortars, extracted from numerical simulations. The dominant principal stresses (σ_{22}) and principal strains (ε_{22}) in the linear elastic range of these systems are used. It is observed from both Figure 5.2 (a) and (b) that effect of debonding is much prominent for a

randomized microstructure than a microstructure containing a single inclusion or four inclusions for a constant volume fraction of inclusions. Thus, a randomized microstructure with varying sizes of the inclusions in the matrix helps bring out the effect of interfacial debonding better than just a single-inclusion or a four inclusion case. While the single-inclusion or four-inclusion systems do show noticeable interfacial debonding, the effect of debonding on the effective composite modulus is much more prominent for the case of randomized microstructure. Combined with the fact that randomized microstructure is inherently realistic, it makes more sense to make use of randomized microstructure when incorporating the effects of debonding in a microstructure. Another observation from Figure 5.3 is that the magnitude of stress inside the quartz particles increases when the particles are very close to each other, attributable to the significant stiffness mismatch between the inclusions and the matrix. Also, in the partially debonded inclusions, prominent stress concentrations are observed where the matrix and the inclusions are still bonded, whereas the recently debonded areas of the matrix show stress relaxations. This is due to the fact that debonding between the matrix and the inclusion tends to redirect the stresses to be imposed on the microstructure based on the stiffness of the component phases in the composite microstructure. Under any kind of loading conditions, the stresses are shared by the matrix and the inclusions in the microstructure based on the stiffness of the individual components of the composite microstructure. When debonding occurs, the interfacial surfaces of the matrix and the inclusions are no longer in contact, which thereby impedes stress transfer between the matrix and the inclusions leading to the stress relaxations as observed in Figure 5.3. The stresses which could not be transferred due to debonding are then redistributed to the nearby contact areas of the matrix and the inclusions

leading to stress concentrations at these locations perpendicular to the direction of debonding under uniaxial loading conditions.

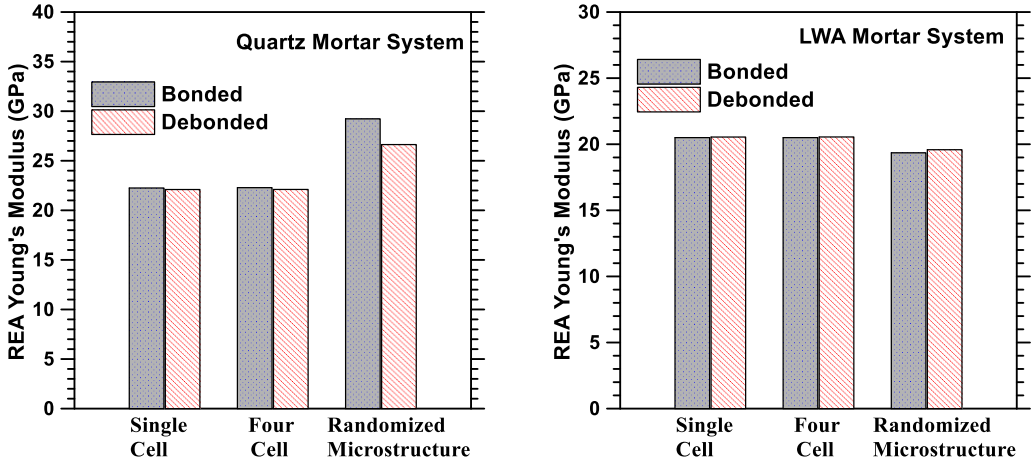

Figure 5.2. Effect of debonding on the REA Young's Modulus for (a) Quartz Mortar System and (b)LWA Mortar System.

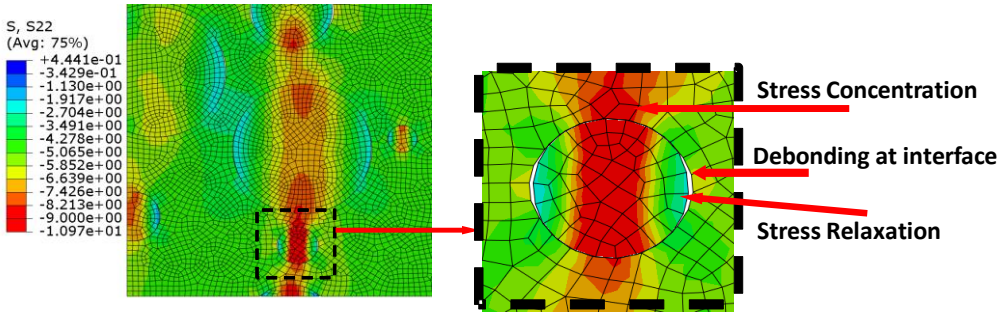

Figure 5.3. Effect of debonding on the stresses in the individual components for a quartz mortar system

The preceding sections have dealt with systems having inclusions without an interfacial transition zone (ITZ). In this section, we study the effect of systems with ITZ on the interfacial debonding occurring at the interface between the ITZ and the inclusion. Figure 5.4 a shows the average principal stress in the quartz mortar with an ITZ for a perfectly bonded case and Figure 5.4 b shows the effect of ITZ on the interfacial debonding and the average principal stress in the quartz mortars respectively. As the ITZ for a quartz

inclusion is generally weaker than the matrix, the stiffness contrast between the inclusion and the ITZ is higher in the quartz-mortar system with an ITZ than in the quartz-mortar system without an ITZ. As such, the debonding index is found to be about 10% higher than in a microstructure having quartz inclusions without an ITZ. The presence of weaker ITZ around a stiffer inclusion leads to increase in the debonding index in the microstructure. As discussed in the previous chapter, for a perfectly bonded case with the presence of ITZ, the stresses are concentrated on the quartz inclusions which are much stiffer than the ITZ. For the case incorporating interfacial debonding, there is visible stress relaxations in the ITZ in the partially bonded regions. The region within quartz inclusion close to the debonded areas also show stress relaxations, whereas stress concentrations are observed in the central region of the quartz inclusion greater than that in the perfectly bonded system. Since the ITZ around a quartz inclusion is generally weaker, it is still likely to fail even though there are regions of stress relaxations.

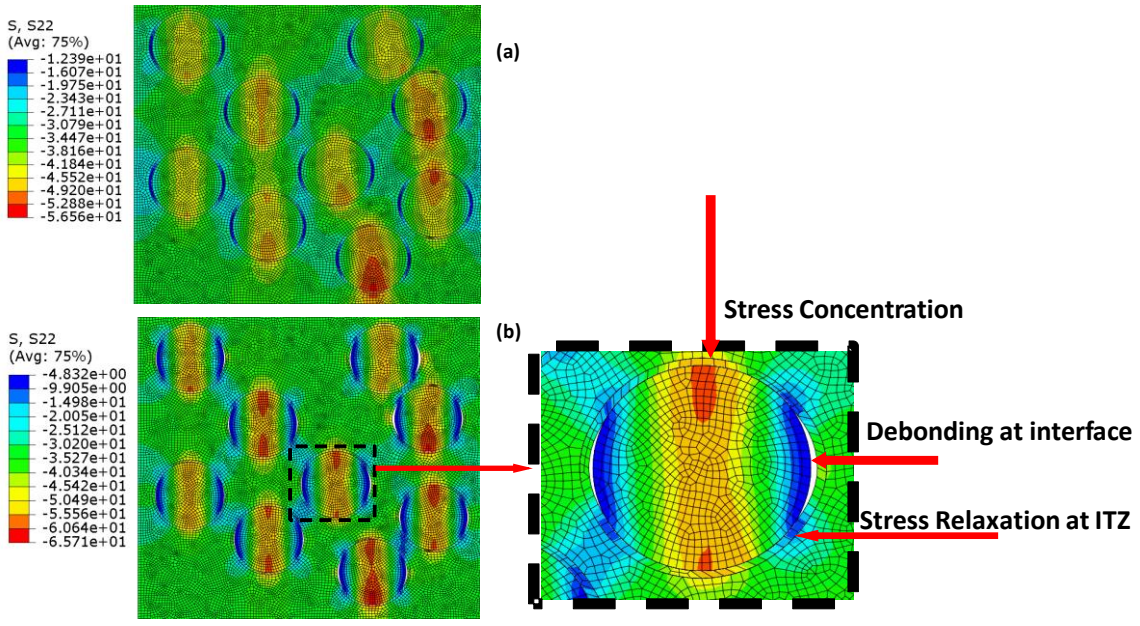

Figure 5.4 Average principal stresses in a quartz mortar with ITZ for (a) Bonded case and (b) Debonded Case

Figure 5.5.a shows the average principal stress in the LWA mortar for a pure bonded case and Figure 5.5.b shows the effect of ITZ on the interfacial debonding and the average principal stress in the LWA mortars respectively. As discussed in the previous chapter, for a pure bonded case with the presence of ITZ, the stresses are concentrated on the ITZ which are stiffer than the inclusions. While for the case incorporating interfacial debonding, there is visible stress concentrations perpendicular to the direction of applied uniaxial loading, in the ITZ in the debonded regions. The region within LWA inclusion close to the debonded areas also show stress relaxations, whereas at the locations of the interfacial debonding prominent stress concentrations are observed in the direction perpendicular to that of the applied strain, where the ITZ and the inclusions are debonded. In the partially bonded regions of the interface stress relaxations are observed in the ITZ. Since the ITZ around a LWA inclusion is generally stiffer and hence stronger, it is unlikely to fail even though there are regions of stress concentrations. Although the presence of an ITZ around an inclusion does affect the stress concentrations and stress relaxations in the microstructure, there is not a significant change in the stress levels. The highest stresses were observed in the stiffest component in both the systems namely quartz inclusion in the quartz mortar system and the ITZ for the LWA mortar system. As such, there is no real advantage of considering ITZ around an inclusion while incorporating interfacial debonding for simulations.

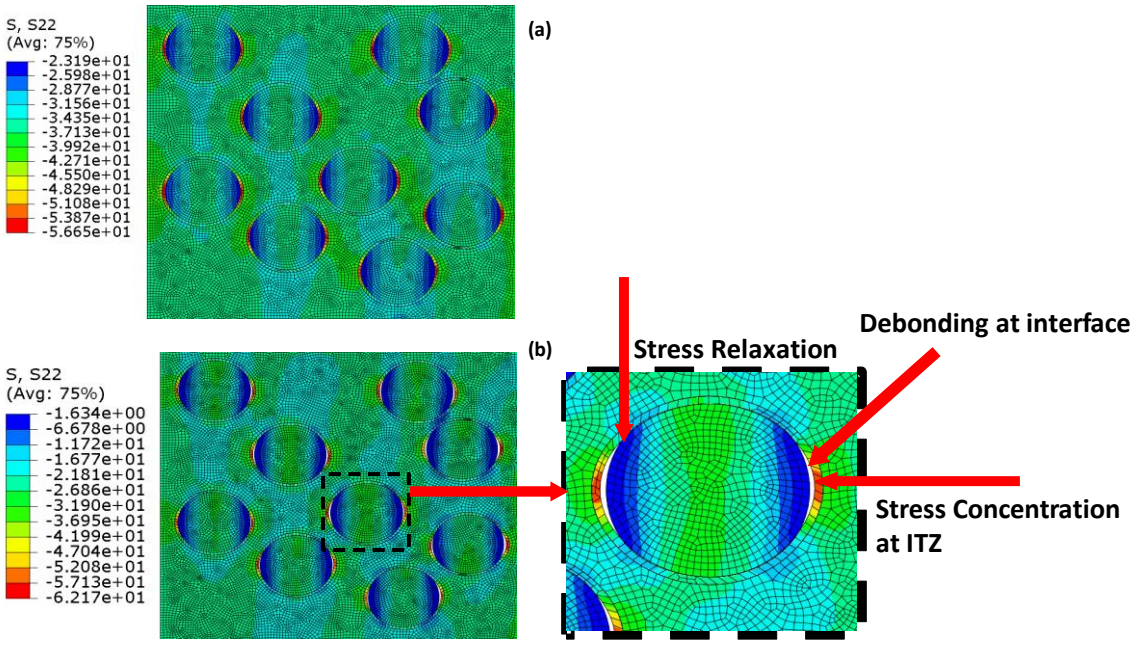

Figure 5.5 Average principal stresses in a LWA mortar with ITZ for (a) Bonded case and (b) Debonded Case

Table 5.1 Composite Young's Modulus for mortars with Quartz and LWA inclusions with and without ITZ for the case of perfectly bonded and debonded systems.

Cement Mortar	Modulus (MPa) With ITZ		Modulus (MPa) Without ITZ	
Inclusion Type	Bonded	Debonded	Bonded	Debonded
Quartz	26664.14	26424.66	27093.74	26781.7
LWA	19901.66	20029.27	19540.09	19625.47

The composite Young's Modulus for cement mortars with quartz and LWA inclusions for the case of perfectly bonded and debonded systems with and without ITZ have been presented in Table 5.1. In the case of debonding with quartz inclusion the composite modulus decreases compared to that of the perfectly bonded case. For quartz mortars containing ITZ the composite modulus is lesser than compared to a quartz mortar without an ITZ for the bonded and the debonded systems. This is to be expected as the ITZ around a quartz mortar is weaker and is quite softer compared to quartz thereby reducing the composite modulus. For the case of debonding with LWA inclusion the composite

modulus increases compared to that of the perfectly bonded case. For LWA mortars containing ITZ the composite modulus is greater than compared to a LWA mortar without an ITZ for the bonded and the debonded systems. This is to be expected as the ITZ around a LWA mortar is stronger and is stiffer than the LWA inclusions thereby increasing the composite modulus.

Figure 5.6 shows the constitutive response of the quartz and LWA mortars containing 30% of inclusions by volume, extracted from numerical simulations. The dominant principal stresses (σ_{22}) and principal strains (ε_{22}) in the linear elastic range of these systems are used to calculate the effective modulus. Thus the approach presented here can be used to determine the composite elastic moduli of systems containing multiple inclusion types while considering the effects of debonding at the interface between the matrix and the inclusions. In addition to the E value, as described earlier, this methodology also provides estimates of the microstresses in the different component phases under imposed strains (in the linear elastic regime) and facilitates the development of constitutive relationships for composite materials, which otherwise would be experimentally tedious. It is reiterated that the models consider the effect of debonding at the interface between the matrix and the inclusions; a case which is more realistic than the models considering perfect bonding. As such models considering debonding help provide more accurate and realistic comparisons of material response with respect to the stress distributions and the constitutive response.

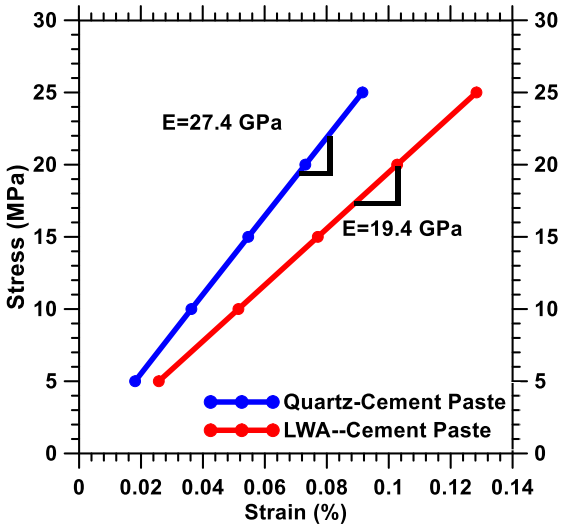

Figure 5.6. Linear constitutive relationship for quartz and LWA mortar systems for defaults values of material parameters (shown in Table 4.1) and microstructural features including debonding.

5.3 Influence of Externally Applied Strain on the Initiation and Propagation of Interfacial Debonding

The effect of externally applied strain on interfacial debonding has been evaluated here using debonding index. The debonding index is defined as the ratio of length of the interface which has debonded to the total length of the interfaces between the matrix and all the inclusions present in the composite microstructure. Figure 5.7 shows the debonding index for both the quartz and the LWA mortar systems, extracted from the numerical simulation. From the figure, it is observed that the debonding index for a quartz inclusion system is greater than that for the LWA inclusion system for all strain levels. Quartz inclusions show significantly higher interfacial debonding due to higher stiffness contrast between the matrix and the inclusions whereas the LWA mortar exhibit lower amount of interfacial debonding due to lower stiffness contrast as compared to the quartz mortar case. The current framework determines the extent of interfacial debonding in a microstructure

which provides valuable information towards design of cementitious composites with various unconventional inclusions for various applications.

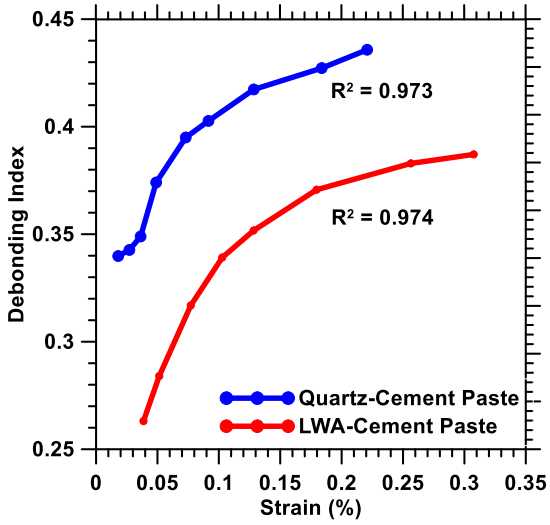

Figure 5.7. Debonding Index for quartz and LWA mortar systems for applied strains.

5.4 Influence of Stiffness of the Inclusions on the Interfacial Debonding

Figure 5.8 shows the debonding index as a function of the varying inclusion stiffness for 30% volume fraction of the inclusion in the microstructure. For a matrix modulus of 20 GPa it is observed that debonding index increases with an increase in the stiffness of the inclusion. The debonding index increases linearly with an increase in the stiffness of the inclusion in the composite microstructure. The debonding index increases with an increase in the stiffness contrast between the inclusions and the matrix. For an inclusion with stiffness of 70GPa the debonding index is about 20% more than the debonding index of an inclusion with a modulus of 16GPa. The higher the contrast in the stiffness between the inclusion and the matrix, greater is the debonding index.

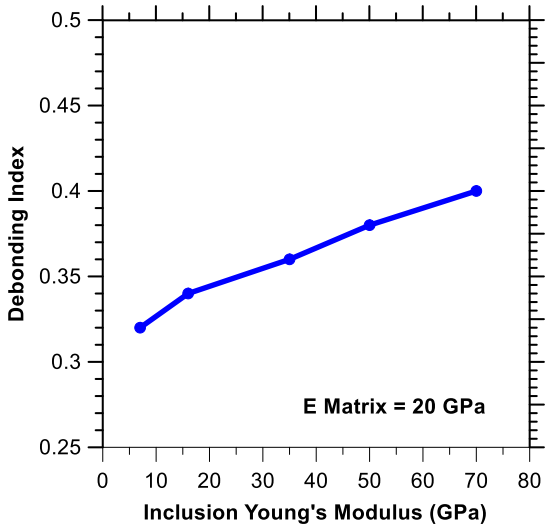

Figure 5.8. Debonding Index for varying inclusion stiffness in a matrix of stiffness 20 GPa.

Chapter 6: Conclusion

The main objective of the present study was to develop a finite element based microstructural model of cementitious composites and study the influence of phase material and geometric properties on the linear elastic constitutive response of the cementitious mortars for both bonded and debonded cases. Finite element analysis gives a better understanding of the microstructural stress distributions between the inclusions and the matrix which contribute significantly to the macroscopic response of the composite.

To generate a realistic finite element model of the composite microstructure, different microstructures and boundary conditions were evaluated. Finally, a randomized periodic geometry along with periodic boundary conditions were selected as the base for all finite element models in this study. The influence of material properties such as inclusions stiffness and matrix stiffening on the stress distributions in the microstructure and the effective modulus of the microstructure were studied. The stresses were concentrated on the quartz inclusion and the matrix for the quartz mortar and light weight aggregate mortar system respectively i.e. the stresses concentrate more in the stiffer component of the respective mortars as expected. The dominant average principal stress for the composite was found to be higher for the quartz mortar than in the LWA mortar. The linear constitutive response for default material properties mentioned in Table 4.1, of the quartz mortar was found to be 31.4 GPa, whereas that of the LWA mortar was found to be 19.6 GPa, values which are in close conformation with those available in literature. For increasing volume fractions of the inclusions the average principal REA stresses in both the systems increase linearly, though the average principal REA stress for the quartz mortar is still higher than that for the LWA mortar system. The highest stresses were observed in

the stiffest component in both the systems namely quartz inclusion in the quartz mortar system and the ITZ for the LWA mortar system. For a microstructure with a mean size of 0.6 mm and standard deviations of 0.06, 0.12, 0.24mm the stress concentrations were observed between closely spaced inclusions especially when aligned perpendicular to the direction of applied strain. For varying particle sizes 20% stress reduction were observed as the interactions between the neighboring inclusions of varying sizes reduces the stresses, contrary to the high stress concentrations encountered between two closely spaced inclusions of similar sizes.

The effective modulus of the composite microstructure obtained from numerical simulations when compared against modulus obtained from the analytical models throw interesting observations. The analytical models (Mori-Tanka, Double Inclusion) predict about 20% & 10% higher value of composite modulus for quartz mortar and LWA mortar systems. Composite modulus obtained from Hobbs's analytical model correlates well with the numerical simulations for low volume fractions. Analytical schemes do not effectively capture the inter-inclusion interactions that result in stress concentrations/relaxations in heterogeneous microstructures. Analytical techniques have been shown to be limited if stiffness contrast between phases is high, as such numerical technique is a much better scheme to obtain the effective composite modulus since it also captures the inter-inclusion interactions mentioned above. Also, a very good correlation is obtained between the numerically predicted and experimentally measured composite modulus which further establishes the viability of using numerical homogenization scheme in determining Young's modulus of heterogeneous microstructures.

The first phase of this thesis focused on the perfectly bonded systems in the linear elastic regime. In the second phase of this thesis, the effect of debonding occurring at the interface between the matrix and the inclusions on the stress distributions in the microstructures is studied. To incorporate the effect of debonding in the finite element models, bilinear softening curve based on traction-separation relationship of quasi brittle material available in literature were adopted. The effect of debonding was checked for a single inclusion, four-inclusion and multiple inclusion system with random microstructure. For the random microstructure a better difference was observed between the bonded and debonded effective composite modulus. As such, randomized microstructure was chosen as a norm for the debonded case of finite element models. The % of debonding of the interfaces was obtained for both quartz and LWA mortar systems when under applied strain. For the quartz mortar system, % debonding is observed to be about 30% more than that for that of LWA mortar systems. With this the extent of debonding in a microstructure can be calculated. When considering ITZ along with debonding in a system, there is visible stress relaxations in the ITZ for the quartz-mortar systems. The highest stresses were observed in the stiffest component namely quartz inclusion in the quartz mortar system. While for the LWA-mortar systems, there are stress concentrations at the ITZ. The highest stresses were observed in the stiffest component in both the systems namely quartz inclusion in the quartz mortar system and the ITZ for the LWA mortar system. For the quartz mortar system, even though there are stress relaxations at the ITZ, since the ITZ is generally quite weak, probability of failure occurring at these locations are still high. While, for the LWA mortar system, even though stress concentrations are observed at the ITZ, since the ITZ is comparatively much stiffer, failure of the system would be dominated

by the soft LWA inclusions. In both systems, failure would be initiated at the softer phases of the heterogeneous microstructure.

The microstructure based numerical homogenization technique accurately captured the stress concentrations in quartz mortar and LWA mortar systems. This resulted in improved predictions of the elastic modulus using the micromechanical scheme, especially for the systems where stiffness contrast between the phases is high, as compared to many analytical homogenization schemes. This study also links the effect of debonding of interfaces in the microstructure with mechanical behavior of two different heterogeneous composites to bring out their fundamental differences in stress distributions and provides valuable input towards material design of cementitious systems with different inclusions of varying stiffness.

REFERENCES

1. Aboudi, Jacob. 1991. “Mechanics of Composite Materials-A Unified Micromechanical Approach.” *NASA STI/Recon Technical Report A* 93: 29778.

2. Ainsworth, Mark. 2001. “Essential Boundary Conditions and Multi-Point Constraints in Finite Element Analysis.” *Computer Methods in Applied Mechanics and Engineering* 190 (48): 6323–39.

3. Akkurt, I., C. Basyigit, S. Kilincarslan, B. Mavi, and A. Akkurt. 2006. “Radiation Shielding of Concretes Containing Different Aggregates.” *Cement and Concrete Composites* 28 (2): 153–57.

4. Al-Jabri, K. S., A. W. Hago, A. S. Al-Nuaimi, and A. H. Al-Saidy. 2005. “Concrete Blocks for Thermal Insulation in Hot Climate.” *Cement and Concrete Research* 35 (8): 1472–79.

5. Axelson, John W., and Edgar L. Piret. 1950. “Crushing of Single Particles of Crystalline Quartz - Application of Slow Compression.” *Industrial & Engineering Chemistry* 42 (4): 665–70.

6. Barenblatt, G.I. 1959. “The Formation of Equilibrium Cracks during Brittle Fracture. General Ideas and Hypotheses. Axially-Symmetric Cracks.” *Journal of Applied Mathematics and Mechanics* 23 (3): 622–36.

7. Bažant, Zdeněk P. 2000. “Size Effect.” *International Journal of Solids and Structures* 37 (1): 69–80.

8. Bažant, Zdeněk P. 2002. “Concrete Fracture Models: Testing and Practice.” *Engineering Fracture Mechanics* 69 (2): 165–205.

9. Bazant, Zdenek P., and Jaime Planas. 1997. *Fracture and Size Effect in Concrete and Other Quasibrittle Materials*. Vol. 16. CRC press.

10. Bažant, Zdeněk P., Qiang Yu, and Goangseup Zi. 2002. “Choice of Standard Fracture Test for Concrete and Its Statistical Evaluation.” *International Journal of Fracture* 118 (4): 303–37.

11. Bentz, D. P., and K. A. Snyder. 1999. “Protected Paste Volume in Concrete: Extension to Internal Curing Using Saturated Lightweight Fine Aggregate.” *Cement and Concrete Research* 29 (11): 1863–67.

12. Bogas, J. Alexandre, and Augusto Gomes. 2013. “Compressive Behavior and Failure Modes of Structural Lightweight Aggregate Concrete – Characterization and Strength Prediction.” *Materials & Design* 46 (April): 832–41.

13. Brassart, L., H. M. Inglis, L. Delannay, I. Doghri, and P. H. Geubelle. 2009. “An Extended Mori–Tanaka Homogenization Scheme for Finite Strain Modeling of Debonding in Particle-Reinforced Elastomers.” *Computational Materials Science,* Proceedings of the 17th International Workshop on Computational Mechanics of MaterialsIWCMM-17, 45 (3): 611–16.

14. Cheeseman, C. R., and G. S. Virdi. 2005. “Properties and Microstructure of Lightweight Aggregate Produced from Sintered Sewage Sludge Ash.” *Resources, Conservation and Recycling* 45 (1): 18–30.

15. Chi, J. M, R Huang, C. C Yang, and J. J Chang. 2003. “Effect of Aggregate Properties on the Strength and Stiffness of Lightweight Concrete.” *Cement and Concrete Composites* 25 (2): 197–205.

16. Chi, Maochieh, and Ran Huang. 2013. “Binding Mechanism and Properties of Alkali-Activated Fly Ash/slag Mortars.” *Construction and Building Materials* 40: 291–98.

17. Cho, Kyu Zong, Albert S. Kobayashi, Neil M. Hawkins, Donald B. Barker, and Fure Lin Jeang. 1984. “Fracture Process Zone of Concrete Cracks.” *Journal of Engineering Mechanics* 110 (8): 1174–84.

18. Cusson, Daniel, and Ted Hoogeveen. 2008. “Internal Curing of High-Performance Concrete with Pre-Soaked Fine Lightweight Aggregate for Prevention of Autogenous Shrinkage Cracking.” *Cement and Concrete Research* 38 (6): 757–65.

19. da Silva, W. R. L., J. Němeček, and P. Štemberk. 2013. “Application of Multiscale Elastic Homogenization Based on Nanoindentation for High Performance Concrete.” *Advances in Engineering Software*, Part I, 62–63 (August): 109–18.

20. Das, Sumanta, Alyson Hendrix, David Stone, and Narayanan Neithalath. 2015. “Flexural Fracture Response of a Novel Iron Carbonate Matrix – Glass Fiber Composite and Its Comparison to Portland Cement-Based Composites.” *Construction and Building Materials* 93 (September): 360–70.

21. Das, Sumanta, David Stone, Barzin Mobasher, and Narayanan Neithalath. 2016. “Strain Energy and Process Zone Based Fracture Characterization of a Novel Iron Carbonate Binding Material.” *Engineering Fracture Mechanics* 156 (May): 1–15.

22. Das, Sumanta, Pu Yang, Sudhanshu S. Singh, James C. E. Mertens, Xianghui Xiao, Nikhilesh Chawla, and Narayanan Neithalath. 2015. “Effective Properties of a Fly Ash Geopolymer: Synergistic Application of X-Ray Synchrotron Tomography, Nanoindentation, and Homogenization Models.” *Cement and Concrete Research*. Accessed September 10.

23. Doghri, Issam, and Amine Ouaar. 2003. “Homogenization of Two-Phase Elasto-Plastic Composite Materials and Structures: Study of Tangent Operators, Cyclic Plasticity and Numerical Algorithms.” *International Journal of Solids and Structures* 40 (7): 1681–1712.

24. Dormieux, Luc, Djimédo Kondo, and Franz-Josef Ulm. 2006. “Drained Microelasticity.” In *Microporomechanics*, 89–135. John Wiley & Sons, Ltd.

25. Drago, Anthony, and Marek-Jerzy Pindera. 2007. “Micro-Macromechanical Analysis of Heterogeneous Materials: Macroscopically Homogeneous vs Periodic Microstructures.” *Composites Science and Technology* 67 (6): 1243–63.

26. Duan, Ping, Zhonghe Shui, Wei Chen, and Chunhua Shen. 2013. “Effects of Metakaolin, Silica Fume and Slag on Pore Structure, Interfacial Transition Zone and Compressive Strength of Concrete.” *Construction and Building Materials* 44 (July): 1–6.

27. Dugdale, D. S. 1960. “Yielding of Steel Sheets Containing Slits.” *Journal of the Mechanics and Physics of Solids* 8 (2): 100–104.

28. Dunant, Cyrille F., Benoît Bary, Alain B. Giorla, Christophe Péniguel, Julien Sanahuja, Charles Toulemonde, Anh-Binh Tran, François Willot, and Julien Yvonnet. 2013. “A Critical Comparison of Several Numerical Methods for Computing Effective Properties of Highly Heterogeneous Materials.” *Advances in Engineering Software* 58 (April): 1–12.

29. Elices, M., G. V. Guinea, J. Gomez, and J. Planas. 2002. “The Cohesive Zone Model: Advantages, Limitations and Challenges.” *Engineering Fracture Mechanics* 69 (2): 137–63.

30. Eshelby, John D. 1957. “The Determination of the Elastic Field of an Ellipsoidal Inclusion, and Related Problems.” In *Proceedings of the Royal Society of London A: Mathematical, Physical and Engineering Sciences*, 241:376–96.

31. Falzone, Gabriel, Guillermo Puerta Falla, Zhenhua Wei, Mingjie Zhao, Aditya Kumar, Narayanan Neithalath, Laurent Pilon, and Gaurav Sant. 2015. “The Influence of Soft and Stiff Inclusions on the Mechanical Properties of Cementitious Composites: Micromechanical Model Predictions.” *Composites: Part A* Under Review.

32. Fernandes, Fabio, Shilpa Manari, Mathew Aguayo, Kevin Santos, Tandre Oey, Zhenhua Wei, Gabriel Falzone, Narayanan Neithalath, and Gaurav Sant. 2014. “On the Feasibility of Using Phase Change Materials (PCMs) to Mitigate Thermal Cracking in Cementitious Materials.” *Cement and Concrete Composites* 51 (August): 14–26.

33. Ghosh, Somnath, Yong Ling, Bhaskar Majumdar, and Ran Kim. 2000. “Interfacial Debonding Analysis in Multiple Fiber Reinforced Composites.” *Mechanics of Materials* 32 (10): 561–91.

34. Gilabert, F. A., D. Garoz, and W. Van Paepegem. 2015. “Stress Concentrations and Bonding Strength in Encapsulation-Based Self-Healing Materials.” *Materials & Design* 67 (February): 28–41.

35. Gopalaratnam, V. S., and Surendra P. Shah. 1985. “Softening Response of Plain Concrete in Direct Tension.” In *Journal Proceedings*, 82:310–23.

36. Goudarzi, Taha, Daniel W. Spring, Glaucio H. Paulino, and Oscar Lopez-Pamies. 2015. “Filled Elastomers: A Theory of Filler Reinforcement Based on Hydrodynamic and Interphasial Effects.” *Journal of the Mechanics and Physics of Solids* 80 (July): 37–67.

37. Grondin, F., H. Dumontet, A. Ben Hamida, G. Mounajed, and H. Boussa. 2007. “Multi-Scales Modelling for the Behaviour of Damaged Concrete.” *Cement and Concrete Research* 37 (10): 1453–62.

38. Grondin, F., and M. Matallah. 2014. “How to Consider the Interfacial Transition Zones in the Finite Element Modelling of Concrete?” *Cement and Concrete Research* 58 (April): 67–75.

39. Guinea, G. V., J. Planas, and M. Elices. 1994. “A General Bilinear Fit for the Softening Curve of Concrete.” *Materials and Structures* 27 (2): 99–105.

40. Gustafsson, P. J., and A. Hillerborg. 1985. “Improvements in Concrete Design Achieved through the Application of Fracture Mechanics.” In *Application of Fracture Mechanics to Cementitious Composites*, 667–80.

41. Hashin, Z., and P. J. M. Monteiro. 2002a. “An Inverse Method to Determine the Elastic Properties of the Interphase between the Aggregate and the Cement Paste.” *Cement and Concrete Research* 32 (8): 1291–1300.

42. Hashin, Z., and P. J. M. Monteiro. 2002b. “An Inverse Method to Determine the Elastic Properties of the Interphase between the Aggregate and the Cement Paste.” *Cement and Concrete Research* 32 (8): 1291–1300.

43. Hashin, Zvi. 1983. “Analysis of Composite Materials—a Survey.” *Journal of Applied Mechanics* 50 (3): 481–505.

44. Hazanov, S. 1998. “Hill Condition and Overall Properties of Composites.” *Archive of Applied Mechanics* 68 (6): 385–94.

45. Hazanov, S., and C. Huet. 1994. “Order Relationships for Boundary Conditions Effect in Heterogeneous Bodies Smaller than the Representative Volume.” *Journal of the Mechanics and Physics of Solids* 42 (12): 1995–2011.

46. Hembade, Lavannya, Narayanan Neithalath, and Subramaniam D. Rajan. 2013. “Understanding the Energy Implications of Phase-Change Materials in Concrete Walls through Finite-Element Analysis.” *Journal of Energy Engineering* 140 (1): 04013009.

47. Hernández-Olivares, F., G. Barluenga, M. Bollati, and B. Witoszek. 2002. “Static and Dynamic Behaviour of Recycled Tyre Rubber-Filled Concrete.” *Cement and Concrete Research* 32 (10): 1587–96.

48. Hillerborg, Arne, Mats Modéer, and P.-E. Petersson. 1976. “Analysis of Crack Formation and Crack Growth in Concrete by Means of Fracture Mechanics and Finite Elements.” *Cement and Concrete Research* 6 (6): 773–81.

49. Hill, Richard. 1952. “The Elastic Behaviour of a Crystalline Aggregate.” *Proceedings of the Physical Society. Section A* 65 (5): 349.

50. Hobbs, D. W. 1971. “The Dependence of the Bulk Modulus, Young’s Modulus, Creep, Shrinkage and Thermal Expansion of Concrete upon Aggregate Volume Concentration.” *Matériaux et Construction* 4 (2): 107–14.

51. Hori, Muneo, and Sia Nemat-Nasser. 1993. “Double-Inclusion Model and Overall Moduli of Multi-Phase Composites.” *Mechanics of Materials* 14 (3): 189–206.

52. Hubert, Jacqueline Sanchez, and Enrique Sanchez Palencia. 1992. *Introduction Aux Méthodes Asymptotiques et à L’homogénéisation: Application à La Mécanique Des Milieux Continus*. Masson.

53. Hu, Chuanlin, and Zongjin Li. 2015. “Property Investigation of Individual Phases in Cementitious Composites Containing Silica Fume and Fly Ash.” *Cement and Concrete Composites* 57 (March): 17–26.

54. Huet, C. 1982. “Universal Conditions for Assimilation of a Heterogeneous Material to an Effective Continuum.” *Mechanics Research Communications* 9 (3): 165–70.

55. Huet, Ch. 1990. “Application of Variational Concepts to Size Effects in Elastic Heterogeneous Bodies.” *Journal of the Mechanics and Physics of Solids* 38 (6): 813–41.

56. Huet, Christian. 1999. “Coupled Size and Boundary-Condition Effects in Viscoelastic Heterogeneous and Composite Bodies.” *Mechanics of Materials* 31 (12): 787–829.

57. Hu, G. K, and G. J Weng. 2000. “The Connections between the Double-Inclusion Model and the Ponte Castaneda–Willis, Mori–Tanaka, and Kuster–Toksoz Models.” *Mechanics of Materials* 32 (8): 495–503.

58. Idiart, M. I., F. Willot, Y. -P. Pellegrini, and P. Ponte Castañeda. 2009. “Infinite-Contrast Periodic Composites with Strongly Nonlinear Behavior: Effective-Medium Theory versus Full-Field Simulations.” *International Journal of Solids and Structures* 46 (18–19): 3365–82.

59. Jiang, M., I. Jasiuk, and M. Ostoja-Starzewski. 2002. “Apparent Elastic and Elastoplastic Behavior of Periodic Composites.” *International Journal of Solids and Structures* 39 (1): 199–212.

60. Jikov, Vasilii Vasil’evich, Sergei M. Kozlov, and Olga Arsen’evna Oleinik. 2012. *Homogenization of Differential Operators and Integral Functionals*. Springer Science & Business Media.

61. Kansal, Anuraag R., Salvatore Torquato, and Frank H. Stillinger. 2002. “Computer Generation of Dense Polydisperse Sphere Packings.” *The Journal of Chemical Physics* 117 (18): 8212–18.

62. Kayali, O. 2008. “Fly Ash Lightweight Aggregates in High Performance Concrete.” *Construction and Building Materials* 22 (12): 2393–99.

63. Ke, Y., A. L. Beaucour, S. Ortola, H. Dumontet, and R. Cabrillac. 2009. "Influence of Volume Fraction and Characteristics of Lightweight Aggregates on the Mechanical Properties of Concrete." *Construction and Building Materials* 23 (8): 2821–28.

64. Ke, Y., S. Ortola, A. L. Beaucour, and H. Dumontet. 2010. "Identification of Microstructural Characteristics in Lightweight Aggregate Concretes by Micromechanical Modelling Including the Interfacial Transition Zone (ITZ)." *Cement and Concrete Research* 40 (11): 1590–1600.

65. Ke, Y., S. Ortola, A. L. Beaucour, and H. Dumontet. 2014. "Micro-Stress Analysis and Identification of Lightweight Aggregate's Failure Strength by Micromechanical Modeling." *Mechanics of Materials* 68 (January): 176–92.

66. Kim, H. K., J. H. Jeon, and H. K. Lee. 2012. "Workability, and Mechanical, Acoustic and Thermal Properties of Lightweight Aggregate Concrete with a High Volume of Entrained Air." *Construction and Building Materials* 29 (April): 193–200.

67. Kitey, R., and H. V. Tippur. 2005. "Role of Particle Size and Filler–matrix Adhesion on Dynamic Fracture of Glass-Filled Epoxy. I. Macromeasurements." *Acta Materialia* 53 (4): 1153–65.

68. Kumar, Aditya, Tandre Oey, Seohyun Kim, Davis Thomas, Sondos Badran, Jialin Li, Fabio Fernandes, Narayanan Neithalath, and Gaurav Sant. 2013. "Simple Methods to Estimate the Influence of Limestone Fillers on Reaction and Property Evolution in Cementitious Materials." *Cement and Concrete Composites* 42: 20–29.

69. Leblanc, Jean L. 2002. "Rubber–filler Interactions and Rheological Properties in Filled Compounds." *Progress in Polymer Science* 27 (4): 627–87.

70. Leblanc, Jean L. 2009. *Filled Polymers: Science and Industrial Applications*. CRC Press.

71. Lee, Seung-Pyo, Ji-Won Jin, and Ki-Weon Kang. 2014. “Probabilistic Analysis for Mechanical Properties of Glass/epoxy Composites Using Homogenization Method and Monte Carlo Simulation.” *Renewable Energy*, SI:AFORE 2012, 65 (May): 219–26.

72. Li, Shuguang. 2008. “Boundary Conditions for Unit Cells from Periodic Microstructures and Their Implications.” *Composites Science and Technology* 68 (9): 1962–74.

73. Löhnert, Stefan. 2004. *Computational Homogenization of Microheterogeneous Materials of Finite Strains Including Damage*. IBNM. http://scholar.google.com/scholar?cluster=10668519372985790217&hl=en&oi=scholarr.

74. Lubachevsky, Boris D. 1991a. “How to Simulate Billiards and Similar Systems.” *Journal of Computational Physics* 94 (2): 255–83.

75. Lubachevsky, Boris D. 1991b. “How to Simulate Billiards and Similar Systems.” *Journal of Computational Physics* 94 (2): 255–83.

76. Lubachevsky, Boris D., and Frank H. Stillinger. 1990a. “Geometric Properties of Random Disk Packings.” *Journal of Statistical Physics* 60 (5-6): 561–83.

77. Lubachevsky, Boris D., and Frank H. Stillinger. 1990b. “Geometric Properties of Random Disk Packings.” *Journal of Statistical Physics* 60 (5-6): 561–83.

78. Lubachevsky, Boris D., Frank H. Stillinger, and Elliot N. Pinson. 1991a. “Disks vs. Spheres: Contrasting Properties of Random Packings.” *Journal of Statistical Physics* 64 (3-4): 501–24.

79. Lubachevsky, Boris D., Frank H. Stillinger, and Elliot N. Pinson. 1991b. “Disks vs. Spheres: Contrasting Properties of Random Packings.” *Journal of Statistical Physics* 64 (3-4): 501–24.

80. Lutz, Melanie P, Paulo J. M Monteiro, and Robert W Zimmerman. 1997. “Inhomogeneous Interfacial Transition Zone Model For The Bulk Modulus Of Mortar.” *Cement and Concrete Research* 27 (7): 1113–22.

81. Makarious, A. S., I. I. Bashter, A. El-Sayed Abdo, M. Samir Abdel Azim, and W. A. Kansouh. 1996. “On the Utilization of Heavy Concrete for Radiation Shielding.” *Annals of Nuclear Energy* 23 (3): 195–206.

82. Malachanne, Etienne, Rita Sassine, Eric Garcia-Diaz, and Frederic Dubois. 2014. “Numerical Model for Mechanical Behavior of Lightweight Concrete and for the Prediction of Local Stress Concentration.” *Construction and Building Materials* 59 (May): 180–87.

83. Meier, H. A., E. Kuhl, and P. Steinmann. 2008a. “A Note on the Generation of Periodic Granular Microstructures Based on Grain Size Distributions.” *International Journal for Numerical and Analytical Methods in Geomechanics* 32 (5): 509.

84. Meier, H. A., E. Kuhl, and P. Steinmann. 2008b. “A Note on the Generation of Periodic Granular Microstructures Based on Grain Size Distributions.” *International Journal for Numerical and Analytical Methods in Geomechanics* 32 (5): 509–22.

85. Miehe, Christian. 2003. “Computational Micro-to-Macro Transitions for Discretized Micro-Structures of Heterogeneous Materials at Finite Strains Based on the Minimization of Averaged Incremental Energy.” *Computer Methods in Applied Mechanics and Engineering* 192 (5): 559–91.

86. Miehe, Christian, Jörg Schröder, and Martin Becker. 2002. “Computational Homogenization Analysis in Finite Elasticity: Material and Structural Instabilities on the Micro-and Macro-Scales of Periodic Composites and Their Interaction.” *Computer Methods in Applied Mechanics and Engineering* 191 (44): 4971–5005.

87. Mier, J. G. M. van. c1997. *Fracture Processes of Concrete : Assessment of Material Parameters for Fracture Models /*. Boca Raton : CRC Press.

88. Miled, K., K. Sab, and R. Le Roy. 2011. “Effective Elastic Properties of Porous Materials: Homogenization Schemes vs Experimental Data.” *Mechanics Research Communications* 38 (2): 131–35.

89. Modéer, Matz. 1979. “A Fracture Mechanics Approach to Failure Analyses of Concrete Materials.” *Report TVBM 1001*. http://lup.lub.lu.se/record/1272886/file/1649662.pdf.

90. Mori, T, and K Tanaka. 1973a. “Average Stress in Matrix and Average Elastic Energy of Materials with Misfitting Inclusions.” *Acta Metallurgica* 21 (5): 571–74.

91. Mori, T, and K Tanaka. 1973b. “Average Stress in Matrix and Average Elastic Energy of Materials with Misfitting Inclusions.” *Acta Metallurgica* 21 (5): 571–74.

92. Mulmule, S. V., and J. P. Dempsey. 1997. “Stress-Separation Curves for Saline Ice Using Fictitious Crack Model.” *Journal of Engineering Mechanics* 123 (8): 870–77.

93. Munjiza, Ante. 2004. *Front Matter*. Wiley Online Library. http://onlinelibrary.wiley.com/doi/10.1002/0470020180.

94. Mura, Toshio. 1987. *Micromechanics of Defects in Solids*. Vol. 3. Mechanics of Elastic and Inelastic Solids. Dordrecht: Springer Netherlands. http://link.springer.com/10.1007/978-94-009-3489-4.

95. Nemat-Nasser, Sia, and Muneo Hori. 2013. *Micromechanics: Overall Properties of Heterogeneous Materials*. Elsevier. https://books.google.com/books?hl=en&lr=&id=wm8vBQAAQBAJ&oi=fnd&pg=PP1&dq=NematNasser,+S.,+and+Hori,+M.+(1999),+Micromechanics:+overall+properties+of+heterogeneous+solids.+2nd+edition.&ots=DWuSZNZj3y&sig=hbxsSBSHs0YLLDZMVlfkIXlqbC8.

96. Nguyen, L. H., A. -L. Beaucour, S. Ortola, and A. Noumowé. 2014. “Influence of the Volume Fraction and the Nature of Fine Lightweight Aggregates on the Thermal and Mechanical Properties of Structural Concrete.” *Construction and Building Materials* 51 (January): 121–32.

97. Nilsen, A. Ulrik, Paulo J. M. Monteiro, and Odd E. Gjørv. 1995. “Estimation of the Elastic Moduli of Lightweight Aggregate.” *Cement and Concrete Research* 25 (2): 276–80.

98. Ostoja-Starzewski, Martin. 1999. “Scale Effects in Materials with Random Distributions of Needles and Cracks.” *Mechanics of Materials* 31 (12): 883–93.

99. Park, Kyoungsoo, Glaucio H. Paulino, and Jeffery R. Roesler. 2008. “Determination of the Kink Point in the Bilinear Softening Model for Concrete.” *Engineering Fracture Mechanics* 75 (13): 3806–18.

100. Park, Kyoungsoo, Glaucio H. Paulino, and Jeffery R. Roesler. 2010. “Cohesive Fracture Model for Functionally Graded Fiber Reinforced Concrete.” *Cement and Concrete Research*40 (6): 956–965.

101. Petersson, P. E. 1981. “Crack Growth and Development of Fracture Zones in Plain Concrete and Similar Structures.” *Report TVBM-1006.(Division of Building Materials, Lund Institute of Technology, Sweden, 1981)*.

102. Qiao, Yu. 2003. “Fracture Toughness of Composite Materials Reinforced by Debondable Particulates.” *Scripta Materialia* 49 (6): 491–96.

103. Ramier, Julien. 2004. “Comportement Mécanique D’élastomères Chargés: Influence de L’adhésion Charge-Polymère: Influence de La Morphologie.” Villeurbanne, INSA. http://www.theses.fr/2004ISAL0028.

104. Reuss, A. 1929. “Berechnung Der Flie\s Sgrenze von Mischkristallen Auf Grund Der Plastizitätsbedingung Für Einkristalle.” *ZAMM-Journal of Applied Mathematics and Mechanics/Zeitschrift Für Angewandte Mathematik Und Mechanik* 9 (1): 49–58.

105. Roelfstra, P. E., and F. H. Wittmann. 1986. “Numerical Method to Link Strain Softening with Failure of Concrete.” *Fracture Toughness and Fracture Energy of Concrete*, 163–75.

106. Roesler, J,PaulinoG. H., Park, K.2007. “Concrete Fracture Prediction Using Bilinear Softening.” *Cement and Concrete Composites*, 29 (4): 300–12.

107. Ruiz, Gonzalo, Michael Ortiz, and Anna Pandolfi. 2000. “Three-Dimensional Finite-Element Simulation of the Dynamic Brazilian Tests on Concrete Cylinders.” *International Journal for Numerical Methods in Engineering* 48 (7): 963–94.

108. Sanahuja, Julien, Luc Dormieux, and Gilles Chanvillard. 2007. “Modelling Elasticity of a Hydrating Cement Paste.” *Cement and Concrete Research* 37 (10): 1427–39.

109. Schröder, Jörg. 2000. “Homogenisierungsmethoden Der Nichtlinearen Kontinuumsmechanik Unter Beachtung von Stabilitätsproblemen.”

110. Segurado, Javier, and Javier LLorca. 2004. “A New Three-Dimensional Interface Finite Element to Simulate Fracture in Composites.” *International Journal of Solids and Structures* 41 (11): 2977–93.

111. Shannag, M. J. 2000. “High Strength Concrete Containing Natural Pozzolan and Silica Fume.” *Cement and Concrete Composites* 22 (6): 399–406.

112. Song, Seong Hyeok, Glaucio H. Paulino, and William G. Buttlar. 2006. “Simulation of Crack Propagation in Asphalt Concrete Using an Intrinsic Cohesive Zone Model.” *Journal of Engineering Mechanics* 132 (11): 1215–23.

113. Stora, E., Q. -C. He, and B. Bary. 2006. “Influence of Inclusion Shapes on the Effective Linear Elastic Properties of Hardened Cement Pastes.” *Cement and Concrete Research* 36 (7): 1330–44.

114. Sun, C. T., and R. S. Vaidya. 1996. “Prediction of Composite Properties from a Representative Volume Element.” *Composites Science and Technology* 56 (2): 171–79.

115. Suquet, Pierre. 1987. “Elements of Homogenization for Inelastic Solid Mechanics.”

116. Terada, Kenjiro, Muneo Hori, Takashi Kyoya, and Noboru Kikuchi. 2000. “Simulation of the Multi-Scale Convergence in Computational Homogenization Approaches.” *International Journal of Solids and Structures* 37 (16): 2285–2311.

117. Thiele, Alexander M., Astrid Jamet, Gaurav Sant, and Laurent Pilon. 2015. "Annual Energy Analysis of Concrete Containing Phase Change Materials for Building Envelopes." *Energy Conversion and Management* 103 (October): 374–86.

118. Torquato, Salvatore. 1991. "Random Heterogeneous Media: Microstructure and Improved Bounds on Effective Properties." *Applied Mechanics Reviews* 44 (2): 37–76.

119. Torquato, Salvatore. 2013. *Random Heterogeneous Materials: Microstructure and Macroscopic Properties*. Vol. 16. Springer Science & Business Media. https://books.google.com/books?hl=en&lr=&id=UTfoBwAAQBAJ&oi=fnd&pg=PR7&dq=Random+heterogeneous+materials:+microstructure+and+macroscopic+properties&ots=w_6ka9R0lV&sig=Mf1il1adGRam8V72_vJ8Ocxc-Zo.

120. Tucker III, Charles L., and Erwin Liang. 1999. "Stiffness Predictions for Unidirectional Short-Fiber Composites: Review and Evaluation." *Composites Science and Technology* 59 (5): 655–71.

121. Van der Sluis, O., P. J. G. Schreurs, W. A. M. Brekelmans, and H. E. H. Meijer. 2000. "Overall Behaviour of Heterogeneous Elastoviscoplastic Materials: Effect of Microstructural Modelling." *Mechanics of Materials* 32 (8): 449–62.

122. Van Rossum, Guido, and others. 2007. "Python Programming Language." In *USENIX Annual Technical Conference*. Vol. 41.

123. Voronoi. 1907. "{Nouvelles Applications Des Paramètres Continus à La Théorie Des Formes Quadratiques}." *Journal Für Die Reine Und Angewandte Mathematik* 133: 97–178.

124. Wasserman, R., and A. Bentur. 1997. "Effect of Lightweight Fly Ash Aggregate Microstructure on the Strength of Concretes." *Cement and Concrete Research* 27 (4): 525–37.

125. Weng, G. J. 1984. "Some Elastic Properties of Reinforced Solids, with Special Reference to Isotropic Ones Containing Spherical Inclusions." *International Journal of Engineering Science* 22 (7): 845–56.

126. Wittmann, F. H., K. Rokugo, E. Brühwiler, H. Mihashi, and Ph Simonin. 1988. "Fracture Energy and Strain Softening of Concrete as Determined by Means of Compact Tension Specimens." *Materials and Structures* 21 (1): 21–32.

127. Wriggers, P., and S. O. Moftah. 2006a. "Mesoscale Models for Concrete: Homogenisation and Damage Behaviour." *Finite Elements in Analysis and Design* 42 (7): 623–36.

128. Wriggers, P., and S. O. Moftah. 2006b. "Mesoscale Models for Concrete: Homogenisation and Damage Behaviour." *Finite Elements in Analysis and Design,* The Seventeenth Annual Robert J. Melosh CompetitionThe Seventeenth Annual Robert J. Melosh Competition, 42 (7): 623–36.

129. Xia, Zihui, Chuwei Zhou, Qiaoling Yong, and Xinwei Wang. 2006. "On Selection of Repeated Unit Cell Model and Application of Unified Periodic Boundary Conditions in Micro-Mechanical Analysis of Composites." *International Journal of Solids and Structures* 43 (2): 266–78.

130. Xu, X.-P., and Alan Needleman. 1994. "Numerical Simulations of Fast Crack Growth in Brittle Solids." *Journal of the Mechanics and Physics of Solids* 42 (9): 1397–1434.

131. Yang, C. C. 1997. "Approximate Elastic Moduli Of Lightweight Aggregate." *Cement and Concrete Research* 27 (7): 1021–30.

132. Yang, C. C. 1998. "Effect of the Transition Zone on the Elastic Moduli of Mortar." *Cement and Concrete Research* 28 (5): 727–36.

133. Yang, C. C., and R. Huang. 1996a. "Double Inclusion Model for Approximate Elastic Moduli of Concrete Material." *Cement and Concrete Research* 26 (1): 83–91.

134. Yang, C. C., and R. Huang. 1996b. "A Two-Phase Model for Predicting the Compressive Strength of Concrete." *Cement and Concrete Research* 26 (10): 1567–77.

135. Yang, Chung-Chia, and Ran Huang. 1998. “Approximate Strength of Lightweight Aggregate Using Micromechanics Method.” *Advanced Cement Based Materials* 7 (3–4): 133–38.

136. Zanjani Zadeh, V., and C. P. Bobko. 2014. “Nanomechanical Characteristics of Lightweight Aggregate Concrete Containing Supplementary Cementitious Materials Exposed to Elevated Temperature.” *Construction and Building Materials* 51 (January): 198–206.

137. Zohdi, Tarek I., and P. Wriggers. 2001. “Computational Micro-Macro Material Testing.” *Archives of Computational Methods in Engineering* 8 (2): 131–228.

138. Zohdi, T. I., and P. Wriggers. 2001. “Aspects of the Computational Testing of the Mechanical Properties of Microheterogeneous Material Samples.” *International Journal for Numerical Methods in Engineering* 50 (11): 2573–99.

139. Zouari, R., A. Benhamida, and H. Dumontet. 2008. “A Micromechanical Iterative Approach for the Behavior of Polydispersed Composites.” *International Journal of Solids and Structures* 45 (11–12): 3139–52.